Geosci. Model Dev. Discuss., doi:10.5194/gmd-2015-239, 2016
Manuscript under review for journal Geosci. Model Dev.
Published: 15 January 2016

Geoscientific Model Development Discussions
Open Access
EGU

Bottom RedOx Model (BROM, v.1.0): a coupled benthic-pelagic model for simulation of seasonal anoxia and its impact

E. V. Yakushev[1,2], E. A. Protsenko[2], J. Bruggeman[3], R. G. J. Bellerby[4,5], S. V. Pakhomova[6,2], R.-M. Couture[1,7], and S. Yakubov[2]

[1]Norwegian Institute for Water Research (NIVA), Gaustadalléen 21, 0349 Oslo, Norway
[2]P. P. Shirshov Institute of Oceanology RAS, Nakhimovskiy prosp. 36, 117991, Moscow, Russia
[3]Plymouth Marine Laboratory, Prospect Place, The Hoe, Plymouth, UK
[4]State Key Laboratory for Estuarine and Coastal Research, East China Normal University, Shanghai, China
[5]Norwegian Institute for Water Research (NIVA Vest), Thormøhlensgate 53 D, 5006 Bergen, Norway
[6]Norwegian Institute for Air Research (NILU), P.O. Box 100, 2027 Kjeller, Norway
[7]University of Waterloo, Earth and Environmental Sciences, Ecohydrology Group, 200 University Avenue West, N2L3G2, Waterloo, Canada

Received: 29 October 2015 – Accepted: 4 December 2015 – Published: 15 January 2016

Correspondence to: E. V. Yakushev (eya@niva.no)

Published by Copernicus Publications on behalf of the European Geosciences Union.

GMDD

doi:10.5194/gmd-2015-239

Abstract

Interaction between seawater and benthic sediments plays an important role in global biogeochemical cycling. Benthic fluxes of chemical elements (C, N, P, O, Si, Fe, Mn, S) directly affect redox state and acidification (i.e. pH and carbonate saturation), which in turn determine the functioning of the benthic and pelagic ecosystems. The redox state of the near bottom layer can change and oscillate in many regions responding to the supply of organic matter, physical regime and coastal discharge. The goal of this work was to develop a model that captures key biogeochemical processes occurring at the bottom boundary layer and sediment–water interface and analyze the changes that result from seasonal variability in redox conditions in the water column. We used a modular approach allowing the model to be coupled to existing hydrophysical models in 1-D, 2-D or 3-D.

The model is capable to simulate seasonality in production and respiration of organic matter as well as in mixing, that leads to variation of redox conditions in the bottom boundary layer. Production and reduction of organic matter and varying redox conditions in the bottom boundary layer affect the carbonate system and lead to changes in pH and alkalinity. Bacteria play a significant role in the fate of organic matter due to chemosynthesis (autotrophs) and consumption of organic matter (heterotrophs). Changes in the bottom boundary layer redox conditions modify the distribution of nutrients (N and P) and redox metals (Mn and Fe). The model can be used for analyzing and interpreting data on sediment-water exchange, and estimating the consequences of forcing such as climate change, external nutrient loading, ocean acidification, carbon storage leakages, and point-source metal pollution.

GMDD

doi:10.5194/gmd-2015-239

1 Background

Oxygen depletion and anoxia are increasingly common features observed in the World Ocean, inland seas and coastal areas. Observations show a decline in the dissolved oxygen concentrations at continental margins in many regions and these are related to both an increase in anthropogenic nutrient loadings and a decrease in vertical mixing e.g., (Diaz and Rosenberg, 2008; Rabalais et al., 2002; Richardson and Jørgensen, 1996). Although bottom waters may be permanently oxic or anoxic, they oscillate seasonally between these extremes in many water bodies (Morse and Eldridge, 2007). Such oscillations typically result from variation in the supply of organic matter (OM) to the sediment–water interface (SWI), from the hydrophysical regime (mixing/ventilation) and nutrient supply (river run-off). Frequently, oxic conditions during periods of intense mixing are followed by near-bottom suboxia or anoxia after the seasonal pycnocline forms, restricting aeration of the deeper layers. This occurs for instance in the Louisiana shelf (Morse and Eldridge, 2007; Yu et al., 2015), Corpus Christi Bay (McCarthy et al., 2008), the Sea of Azov (Debolskaya et al., 2008), and Elefsis Bay (Pavlidou et al., 2013).

The redox state and oxygenation of near-bottom water is directly affected by transport of oxidized and reduced species across the SWI and, consequently, by biogeochemical processes occurring in the sediment itself (Cooper and Morse, 1996; Jorgensen et al., 1990; Roden and Tuttle, 1992; Sell and Morse, 2006). The sediment generally consumes oxygen due to enrichment with OM and presence of reduced forms of chemical elements. Its capacity to exchange oxygen with the pelagic is limited, as near bottom water is usually characterized by lowwater velocity and reduced mixing in the vicinity of the SWI (Glud, 2008). In combination, a high benthic oxygen demand (BOD) associated with local OM mineralization and low mixing rates can cause anoxia in the bottom water. This leads to the death or flight of benthic macro and meio faunal organisms responsible for bioturbation and bioirrigation (Blackwelder et al., 1996; Sen Gupta et al., 1996; Morse and Eldridge, 2007), which can greatly slow down the

GMDD
doi:10.5194/gmd-2015-239

transport of solid and dissolved species inside the sediments and therefore rates of oxidative reactions there. Under such conditions, sedimentary sulphides can build up and dissolution of carbonate minerals may come to a halt (Morse and Eldridge, 2007).

A large number of studies demonstrate the capabilities of sophisticated reactive transport codes for integrated modelling of biogeochemical cycles in sediments e.g. (Paraska et al., 2014). However, few have directly investigated the influence of variable redox conditions in the water column on the depth-distribution of biogeochemical processes (Katsev and Dittrich, 2013; Katsev et al., 2007) which thus remains an open question.

When oxic conditions return, there can be an "oxygen debt" of reduced species in the water column (Yakushev et al., 2011) and at the sediment–water interface this may buffer and delay the reestablishment of oxygenation to the sediments (Morse and Eldridge, 2007). In areas experiencing seasonal hypoxia/anoxia, the processes taking place in the water column and in the sediments are thus tightly coupled. Predicting the occurrence of hypoxia/anoxia thus requires a quantitative understanding of the dynamics of the network of physical, chemical and biological processes occurring in these environments, which drive oscillating redox conditions. Consequently, sophisticated fully coupled physical–biogeochemical models have established themselves as powerful tool to address this gap (Yu et al., 2015), although the tools are however often site-specific and complex to set-up. Furthermore, the Bottom Boundary Layer (BBL) – a thin layer of water within which the steepest gradients and the greatest fluctuations in redox conditions are occurring, is still understudied.

The goal of this work was to develop a model that captures key biogeochemical processes occurring at the BBL and analyse the changes that result from seasonal variability in redox conditions in the water column.

GMDD
doi:10.5194/gmd-2015-239

2 Model description

Here we present the one-dimensional vertical transport and reaction model Bottom RedOx Layer Model, BROM. BROM builds on ROLM (RedOx Layer Model), a model constructed to simulate basic biogeochemical structure of the water column oxic/anoxic interface in the Black and Baltic Seas and fjords (Yakushev et al., 2006, 2007, 2009, 2011; He et al., 2012; Stanev et al., 2014). We extended the biogeochemical module of the model to consider an extensive list of compounds and processes (Fig. 1), although this paper focuses on description of the fate of the species of the most important elements affected by the changes of the redox conditions – oxygen (O), nitrogen (N), sulphur (S), manganese (Mn), iron (Fe) – and describe the concurrent and resultant changes in the alkalinity and carbonate systems. The biogeochemical module of BROM includes parameterizations of OM production (via photosynthesis and chemosynthesis) and decay, and the transformation of phosphorus and silicate. BROM also includes a module describing the carbonate equilibria to account for the dynamic behavior of the components of total alkalinity significant in suboxic and anoxic conditions (i.e. speciation of S, N, Si, P).

The physical domain of the model spans the water column, the BBL and the upper layer of the sediments in a continuous fashion. That allowed moving the boundary conditions as far as possible from the place of interest, the sediment water interface, i.e. to the water/air boundary and deep in the sediment.

To parameterize the water column, including temperature, salinity and turbulent diffusivity, we use results of a simulation of turbulent mixing performed using the General Ocean Turbulence Model (GOTM) (Bolding et al., 2002) for the North Sea. In the limits of the BBL, mixing was assumed to be constant. In the sediments, molecular diffusion and bioirrigation/bioturbation were parameterized.

BROM is built upon an existing modular platform (Framework for Aquatic Biogeochemical Modelling-FABM, Bruggeman and Bolding, 2014) and present a mechanistic biogeochemical model that formalizes universal principles that apply throughout all

GMDD
doi:10.5194/gmd-2015-239

three domains considered: pelagic, the BBL and upper sediment. BROM is written as set of reusable components, consisting consists of a stand-alone transport driver and separate modules for ecology, redox chemistry and carbonate chemistry. These modules are reusable: the transport driver can be used with all other biogeochemical models available in FABM, including the European Regional Seas Ecosystem Model (ERSEM), and BROM biogeochemical modules can be used in all other 1-D and 3-D hydrodynamic models supported by FABM (e.g., GOTM, GETM, MOM5, NEMO, FV-COM). Individual BROM modules can also be coupled to existing ecological models to expand their feature set, e.g., by providing them with descriptions of redox and carbonate chemistry. Via FABM, this approach allows transparent setup of a complex biogeochemical reaction network for the prediction of hypoxia/anoxia while harnessing the capabilities of various hydrophysical drivers. This allows an investigation of the dynamics of interfaces in the water column-sediment continuum that is critical for ecosystem functioning, yet hard-to-reach for in-situ exploration.

This presented model application can be considered as rather theoretical one aiming in analyses of the potential influence of the changeable redox conditions on the properties distributions and processes rates. Here we present model results for the seasonal variability of biogeochemical variables, emerging from the interplay of modelled biogeochemical processes, the variability in environmental conditions (temperature, salinity, turbulent mixing), and the imposed boundary conditions (prescribed constant concentrations or fluxes for selected variables).

2.1 Biogeochemical module

2.1.1 General description

BROM contains 3 biogeochemical modules: BROM_bio (ecological model), BROM_redox (redox processes) and BROM_carb (carbonate system).

In BROM, reactions are either defined as kinetic processes (e.g. organic matter degradation) or protolithic processes (e.g. carbonate system equilibration) (Boudreau,

GMDD
doi:10.5194/gmd-2015-239

1996; Jourabchi et al., 2008; Luff et al., 2001). In general, the protolythic reactions are fast compared to other kinetic processes and compared to the time step at which the model is typically integrated. Therefore, equilibrium concentrations of the chemical element species involved in such reactions can be calculated using mass action laws and equilibrium constants for the seawater (Millero, 1995). That takes away the need to include a separate state variable for e.g. pH, which instead is calculated as a diagnostic at every time step as a function of DIC and Alk (that are state variables). In turn, pH is then used in calculations of the chemical equilibrium constants required to describe related processes (i.e. carbonate precipitation/dissolution, carbonate system parameters etc.).

The model state variables (C_i) are described in Table 1.

The simplified ecological model of BROM reflects main functional groups of organisms (i.e. phytoplankton, heterotrophs, 4 functional groups of bacteria, aerobic heterotrophic, aerobic autotrophic, anaerobic heterotrophic, anaerobic autotrophic) and parameterizes the key features of organic matter production and decomposition, which is based on Redfield and Richards stoichiometry (Richards, 1965).

The model contains frequently measured components such as sulfides (H_2S) and phosphate (PO_4) whose spatial and temporal variability is generally known, as well as rarely measured variables such as elemental sulfur (S^0), thiosulfate (S_2O_3), trivalent manganese species Mn(III) and bacteria. Variables of the latter category were included because their contribution to biogeochemical transformations is believed to be substantial. For instance, bacteria play an important role in many of the processes modelled and can consume or release nutrients as in both the organic and inorganic form Canfield et al. (2005) and Kappler et al. (2005). The equations and parameters employed in BROM are given in Tables 2 and 3, a flow chart is shown in Fig. 1.

2.1.2 Ecosystem and redox model

The BROM model of ecosystem and redox processes are equivalent to those featured in ROLM. The main goal of the ecosystem parameterization is to describe the fate of

GMDD
doi:10.5194/gmd-2015-239

OM. OM is produced photosynthetically by phytoplankton and chemosynthetically by bacteria, specifically by aerobic autotrophic bacteria in oxic conditions and by anaerobic autotrophic bacteria in anoxic conditions. Growth of heterotrophic bacteria is tied to mineralization of OM, favouring aerobic bacteria in oxic conditions and anaerobic bacteria in anoxic conditions. Heterotrophs consume phytoplankton, all types of bacteria and detritus. The effect of suboxia and anoxia is parameterized by letting the mortality of aerobic organisms depend on the oxygen availability.

Mineralization of OM leads to a consequent depletion of oxygen, nitrate, oxidized Mn, oxidized Fe and sulfate. The redox processes that affect reduced and oxidized inorganic species of nitrogen, sulphur, manganese and iron, and phosphorus species are also parameterized. A detailed description of this processes and parameterizations is given in Yakushev at al. (2007, 2013).

2.1.3 Total alkalinity

Total alkalinity, A_T, is a model state variable. Following the formal definition of A_T (Dickson, 1992; Wolf-Gladrow et al., 2007; Zeebe and Wolf-Gladrow, 2001) the following alkalinity components are considered:

$$A_T = A_{TCO_2} + A_B + A_{TPO_4} + A_{Si} + A_{TNH_3} + A_{TH_2S} + [OH^-] - A_{THF} - A_{THNO_2} - A_{TSO_4} - [H^+] + A_{TOM}$$

where the carbonate alkalinity, $A_{TCO_2} = [HCO_3^-] + 2[CO_3^{2-}]$, the phosphoric alkalinity, $A_{TPO_4} = [HPO_4^{2-}] + 2[PO_4^{3-}]$, the ammonia alkalinity, $A_{TNH_3} = [NH_3] + [NH_4^+]$, the silicic alkalinity $A_{Si} = [H_3SiO_4^-]$, and the hydrogen sulphide alkalinity, $A_{TH_2S} = [HS^-]$, are calculated from the corresponding model state variables (Table 1) according to (Luff et al., 2001; Volkov, 1984). The boric alkalinity, $A_B = [B(OH)_4^-]$, is estimated from salinity. Hydrogen sulfate alkalinity, $A_{TSO_4} = [HSO_4^-]$, nitrous acid alkalinity $A_{THNO_2} = [HNO_2]$ and the hydrofluoric alkalinity, $A_{THF} = [F^-] + [HF]$, were ignored due to their insignificant role

GMDD
doi:10.5194/gmd-2015-239

to the A_T variations in this study. A_{TOM}, the alkalinity connected with total (dissolved and particulate) organic matter, TOM, was assumed set to 0.

Biogeochemical processes can affect alkalinity via the "nutrient-H^+ compensating principle" formulated by Wolf-Gladrow et al. (2007): during uptake or release of charged nutrient species, electroneutrality is maintained by consumption or production of proton (i.e. during uptake of nitrate for photosynthesis or denitrification, or production of nitrate by nitrification). Besides these, the biogeochemical process can lead to either increase or decrease of alkalinity, and alkalinity can be used as indicator of specific biogeochemical processes (Soetaert et al., 2007).

The effect on alkalinity of the following redox reactions occurring in suboxic and anoxic conditions via production or consumption of $[OH^-]$ and $[H^+]$ or changes of "standard" alkalinity components was explicitly considered in the model:

$$4Mn^{2+} + O_2 + 4H^+ \rightarrow 4Mn^{3+} + 2H_2O$$

$$2Mn^{3+} + 3H_2O + 0.5O_2 \rightarrow 2MnO_2 + 6H^+$$

$$2MnO_2 + 7H^+ + HS^- \rightarrow 2Mn^{3+} + 4H_2O + S^0$$

$$2Mn^{3+} + HS^- \rightarrow 2Mn^{2+} + S^0 + H^+$$

$$Mn^{2+} + HS^- \leftrightarrow MnS + H^+$$

$$Mn^{2+} + CO_3^- \leftrightarrow MnCO_3$$

$$2MnCO_3 + O_2 + 2H_2O \rightarrow 2MnO_2 + 2HCO_3^- + 2H^+$$

$$4Fe^{2+} + O_2 + 10H_2O \rightarrow 4Fe(OH)_3 + 8H^+$$

$$2Fe^{2+} + MnO_2 + 4H_2O \rightarrow 2Fe(OH)_3 + Mn^{2+} + 2H^+$$

$$2Fe(OH)_3 + HS^- + 5H^+ \rightarrow 2Fe^{2+} + S^0 + 6H_2O$$

$$Fe^{2+} + HS^- \leftrightarrow FeS + H^+$$

$$FeS + 2.25O_2 + 2.5H_2O \rightarrow Fe(OH)_3 + 2H^+ + SO_4^{2-}$$

$$FeS_2 + 3.5O_2 + H_2O \rightarrow Fe^{2+} + 2SO_4^{2-} + 2H^+$$

GMDD
doi:10.5194/gmd-2015-239

$$4S^0 + 3H_2O \rightarrow 2H_2S + S_2O_3^{2-} + 2H^+$$
$$NH_4^+ + 1.5O_2 \rightarrow NO_2^- + 2H^+ + H_2O$$
$$0.75CH_2O + H^+ + NO_2^- \rightarrow 0.5N_2 + 1.25H_2O + 0.75CO_2$$
$$4S^0 + 3H_2O \rightarrow 2H_2S + S_2O_3^{2-} + 2H^+$$
$$2S^0 + O_2 + H_2O \rightarrow S_2O_3^{2-} + 2H^+$$
$$4S^0 + 3NO_3^- + 7H_2O \rightarrow 4SO_4 + 3NH_4^+ + 2H^+ S_2O_3^{2-} + 2O_2 + OH^- \rightarrow 2SO_4^{2-} + H_2O$$
$$3H_2S + 4NO_3^- + 6OH^- \rightarrow 3SO_4^{2-} + 2N_2 + 6H_2O$$
$$Ca^{2+} + CO_3^2 \leftrightarrow CaCO_3$$

There were also parameterized changes in the "standard" alkalinity components (i.e. A_{TNH_3}, A_{TH_2S}) followed from these reactions and all the other reactions considered in the model (Table 3).

2.1.4 Carbonate system

Equilibration of the carbonate system was considered as a fast process occurring in less than several seconds (protolithic reactions) (Zeebe and Wolf-Gladrow, 2001). Accordingly, the equilibrium solution was calculated at every time step using an iterative procedure. That was needed to model the fate of, for example, calcium carbonate that is involved in both protolithic reactions and with transport processes. The carbonate system was described using standard approaches (Lewis and Wallace, 1998; Roy et al., 1993; Wanninkhof, 2014; Wolf-Gladrow et al., 2007; Zeebe and Wolf-Gladrow, 2001). We used Roy's set of constants (Roy et al., 1993), total pH was calculated using the Newton–Raphson method. Precipitation and dissolution of calcium carbonate were modeled following an approach of (Luff et al., 2001) (Table 2).

GMDD
doi:10.5194/gmd-2015-239

2.2 Physical environment

The 1-dimensional model domain spans the water column, the Bottom Boundary Layer (BBL) and the upper layer of the sediments.

The water column extends from 0 to 90 m (with a spatial resolution of 5 m), the BBL from 90 to 90.5 m (with a spatial resolution of 2.5 cm) and the upper layer of sediments from 90.5 to 90.62 m (with a spatial resolution of 2 mm). This rather thick BBL was taken to illustrate the peculiarities of the biogeochemical structure above the bottom in case of bottom anoxic formation.

The time space evolution of the BROM biogeochemical variables is described by a system of horizontally integrated vertical diffusion equations for non-conservative substances:

$$\frac{\partial C_i}{\partial t} = \frac{\partial}{\partial z} K_z \frac{\partial C_i}{\partial z} - \frac{\partial (W_{Ci} + W_{\mathrm{Me}}) C_i}{\partial z} + R_{C_i} \quad (1)$$

where C_i – concentration of a model compounds; K_z – vertical transport coefficient; W_{Ci} is the sinking rate of the particulate matter; W_{Me} – sinking rate of particles with settled Mn and Fe hydroxides; $R_{C_i} = \sum_j R_{\mathrm{B}_j C_i}$ – combined sources minus sinks of a substance (rates of transformation), being an algebraic sum of terms associated with specific biogeochemical processes ($R_{\mathrm{B}_j C_i}$).

To evaluate the behaviour of the model under realistic forcing we use North Sea data (Bolding et al., 2002) to parameterize water column characteristics and to test on an independent subset of the data results of the biogeochemical model. Data for water column parameterization include initial profiles of temperature and salinity, external pressure gradients (e.g., tidal constituents), and surface forcing. Data used to evaluate model results include the fluxes and concentrations in the sediments, as well as additional observations (i.e. local presence of the bacterial mats). The mathematical parameterization of the vertical exchange treats K_z as the turbulent diffusion coefficient

GMDD
doi:10.5194/gmd-2015-239

in the water column and molecular diffusion coefficient in the sediments. Bioirrigation and bioturbation can also be parameterized as modifiers of the value of K_z

To the water column K_z is provided by the results of the 1-D General Ocean Turbulence Model (GOTM) simulations for the Northern North Sea, described in (Bolding et al., 2002) http://www.gotm.net/index.php?go=software&page=testcases. We aimed for a solution representative for "present day", and we are thus treating the GOTM setup incl. forcing as representative for a "normal year".

For the BBL K_z was assumed to be constant with value $0.5 \times 10^{-6}\,m^2\,s^{-1}$.

In the sediments, K_z was parameterized as a sum of the pore water molecular diffusion coefficient $K_{z\_mol} = 1 \times 10^{-11}\,m^2\,s^{-1}$ and bioirrigation/bioturbation coefficient.

Bioturbation activity (i.e. mixing of sediment particulates by burrowing infauna) and bio-irrigation (i.e. flushing of benthic sediment by burrowing fauna through burrow ventilation) were parameterized in the model. In mesocosm experiments with North Sea sediments (Queirós et al., 2014) the biodiffusion coefficient was found to be 2–5 $cm^2\,yr^{-1}$ (0.6–1.6 $\times 10^{-11}\,m^2\,s^{-1}$) and the maximum bioturbation depth was 0.5–2.2 cm. In current version of model sediment porosity is not explicitly considered, but its effect on vertical transport is incorporated in the values of K_z and K_{z_bio}, which together control the vertical diffusion in the sediment. K_z is set to a constant value of $1.10^{-11}\,m^2\,s^{-1}$, it was calculated using averaged substance-dependent diffusion coefficient (Boudreau, 1997) adjusted by assuming a constant porosity of 90 % (applicable for upper 10 cm of sediment, Vershinin, Rozanov, 2002) and by a tortuosity corresponding to this porosity value (value from Boudreau, 1997). K_{z_bio} is a value of biodiffusion coefficient, it is constant for upper 2 cm of sediment ($K_{z\_bio\_max} = 1.10^{-11}\,m^2\,s^{-1}$) and further exponentially decrease with depth. K_{z_bio} is further scaled with a Michaelis–Menten function of the oxygen concentration.

$$K_{z\_bio} = K_{z\_bio\_max} \frac{O_{2s}}{O_{2s} + K_{O_{2s}}} \quad (2)$$

GMDD
doi:10.5194/gmd-2015-239

Where O_{2s} is the concentration of dissolved oxygen at the sediment surface, $K_{z\_bio\_max}$ is maximum bioturbation/bioirrigation coefficient and $K_{O_{2s}} = 1\,\mu M$ is a constant.

Constant W_{Ci} values were assumed for phytoplankton, zooplankton, bacteria, and detritus (Table 3). In addition, the effect of increased sinking rates due to the formation of Mn(IV) and Fe(III) oxides and their association with particulate organic matter (POM) was parameterized. It was found that the precipitation of particulate Mn oxide significantly increases the flux of sinking particles, which, in turn, affects the overall distribution of particles (Yakushev and Debolskaya, 2000):

$$W_{Me} = W_{Me}^{max} \frac{Mn(IV)}{Mn(IV) + K_{Me}} \quad (3)$$

Coefficients W_{Me}^{max} and K_{Me} are given in Table 3.

2.3 Boundary conditions

The water column considered in our model spans the sea surface (upper boundary) down to user's defined sediment depth (12 cm depth in this application) as a lower boundary. At the upper boundary, fluxes of the modeled chemical constituents are assumed to be zero, with the exception of O_2, CO_2, PO_4, inorganic nitrogen compounds and Fe and Mn oxides.

For oxygen, the surface flux represents exchange with the atmosphere. This is given by the flux equation:

$$Q_{O_2} = k_{660}(Sc/660)^{-0.5}(Oxsat - O_2), \quad (4)$$

where Oxsat is equal to oxygen saturation as a function of temperature and salinity, according to UNESCO (1986); Sc is the Schmidt number; k_{660} is the reference gas-exchange transfer velocity. To describe k_{660} as a function of wind speed, the following equation is used:

$$k_{660} = 0.365u^2 + 0.46u \quad (5)$$

GMDD
doi:10.5194/gmd-2015-239

Simulations are carried out using a mean wind speed $u = 5\,\mathrm{m\,s^{-1}}$.

CO_2 exchange was parameterized in a same way as for oxygen, with atmospheric CO_2 equal 400 ppm during all the seasons, but with a different Sc.

Inputs of phosphorus, nitrogen, iron and manganese from atmospheric precipitates and rivers were taken into account by prescribing concentrations at the sea surface. For phosphorus (Q_P) and nitrogen (Q_N), the seasonality in these inputs was considered by imposing time-varying surface concentrations:

$$\mathrm{Conc}(PO_4) = (1 + \sin(2\pi \times (\mathrm{julianday} + 55)/365)) \times 0.9 \quad (6)$$

$$\mathrm{Conc}(NO_3) = (1 + \sin(2\pi \times (\mathrm{julianday} + 55)/365)) \times 7 \quad (7)$$

where julianday is the Julian day number.

Constant surface concentrations were prescribed for the following variables: SO_4 (25×10^{-3} µM), Alk (2250 µM), Mn(IV) (1×10^{-4} µM), Fe (III) (5×10^{-5} µM). At the lower boundary we assumed constant concentrations of SO_4 (25×10^{-3} µM). Therefore, the model biogeochemistry was predominantly forced by the upper boundary conditions; the concentrations at the lower boundary emerge as a result of processes occurred in the water column, BBL and upper sediment. The boundary conditions for the physical parameters used in the model were those described in (Bolding et al., 2002). Irradiance was calculated as described in Table 3.

2.4 Computational aspects

Numerical integration was conducted with the Eulerian scheme and by process splitting (i.e., separate treatment of diffusion, advection/sinking and reaction/source-sink terms). Time steps were set to 2.5×10^{-3} d for biogeochemical processes and sinking and 6.25×10^{-4} d for diffusion, that is 54 s, a much larger number that the characteristic scale of the CO_2 kinetics (Zeebe and Wolf-Gladrow, 2001). The initial calculations assume a vertically homogenous distribution of all biogeochemical variables, with compound-specific initial concentrations. To subsequently resolve spatial and temporal

GMDD
doi:10.5194/gmd-2015-239

variation in the biogeochemical components, calculations are repeated with seasonal changes of temperature, salinity, vertical turbulence in the water column (calculated with GOTM) and irradiance until a quasi-stationary solution with seasonal forced oscillations of the biogeochemical variables is reached. The code is written in FORTRAN and was run with the Intel FORTRAN for Windows Compiler.

To determine the vertically balanced distribution, the calculations were repeated with seasonal changes of temperature, salinity, vertical turbulence in the water column (calculated with GOTM) and irradiance until a quasi-stationary solution with seasonal forced oscillations of the biogeochemical variables was reached. That is, there were no changes in the year-averaged concentrations of the variables for at least 100 model-years.

3 Model output discussion

In this work we used a simplified hydrodynamic scenario, since the main goal of the model was to reproduce the biogeochemical mechanism of transformation of oxic conditions into anoxic in the sediment–water interface. The model biogeochemical modules consider relatively fast processes, (seasonal and shorter), and therefore exclude longer time scale processes, occurring on e.g. geological time scales. Additionally, the model was forced only at the sea surface and did not include fluxes of reduced components (i.e. hydrogen sulphide, Mn(II), MnS, FeS) across the low boundary of the model, in order to focus exclusively on the consequences of supply of the fresh organic matter as a main reducer in the water column and in the sediments.

3.1 Test case simulations

The model shows a possibility of the periodic replacement of oxic conditions with anoxic, which leads to changes in the vertical distributions of the biogeochemical vari-

GMDD
doi:10.5194/gmd-2015-239

ables (Figs. 2–6) and their fluxes (Fig. 7). These simulations revealed a number of characteristic features of the sediment water interface biogeochemistry.

In the oxygenated winter period the oxic/anoxic interface was positioned at several millimeters depth in the sediments (see also Fig. 2). Deposition of large amounts of OM to the bottom under restricted oxygen supply leads to a shift of this interface toward the sediment surface, due to consistent consumption of O_2, NO_3, Mn(IV), Mn(III), Fe(III) and SO_4 for the OM mineralization (Fig. 4). In the BBL O_2 started to disappear in the middle of summer, accompanied by slower remineralization of OM and slower oxidation of reduced forms of Mn, N, Fe and S. After O_2 consumption, NO_3 became a dominant oxidizer, which was then also rapidly depleted.

After the decrease of oxygen at the sediment–water interface to 5 µM, the release from the bottom of S_2O_3 and S^0 starts; hydrogen sulphide initially remains in the sediments, only to enter the water column several days later (Fig. 4). This is explained by the significant concentrations of Mn and Fe oxides in the upper millimeters of the sediments which prevented the immediate release of H_2S. Mn and Fe oxides react with hydrogen sulphide producing S_2O_3 and S^0. The modelled order of appearance in the water column of the intermediate sulphur species (first S_2O_3, then S^0 and then H_2S) corresponds to their typical order of appearance at real water column redox interfaces (Kamyshny et al., 2013). The delayed release of H_2S allowed the bottom surface and the BBL to be in suboxic conditions, allowing the accumulation of Mn(III).

Total dissolution of Fe and Mn oxides in late summer leads to a release of the H_2S from the sediments and an upward shift of the oxic/anoxic interface into the water column (Fig. 6). This is accompanied by the disappearance of the phosphate minimum at the sediment surface (connected with trapping by the metal oxides) and sudden influx of phosphate from the sediment into the water. The calculated seasonal variability of the vertical fluxes (Fig. 7) illustrates this behavior and allows us to compare roles of different species affecting the position of the redox interface.

During the anoxic period, H_2S, Mn(II), PO_4, Fe(II), S_2O_3 and NH_4 move upward in the water-sediment column (Fig. 7).

GMDD
doi:10.5194/gmd-2015-239

The majority of occurring redox processes is microbially mediated, leading to bacterial growth (both heterotrophs and autotrophs) and production of new OM (by autotrophs). This forms a positive feedback that accelerates the consumption of oxidizing compounds.

After the formation of suboxic and anoxic conditions in the BBL, aerobic heterotrophic bacteria disappear and an increase of the aerobic autotrophic and anaerobic heterotrophic bacteria is seen. This modelled increase of the bacterial concentrations at the sediment surface could hint at the presence of bacterial mats, which are known to occur under hypoxic/anoxic conditions [REF].

Winter flushing events lead to an abrupt increase of O_2 above the bottom, the appearance of Mn(IV), Mn(III) and Fe(III) in the water column, and their accumulation at the sediment surface (Fig. 5). This is followed by a deepening of the oxic/anoxic interface inside the sediments during the winter.

The model clearly demonstrates the presence of a fine vertical biogeochemical structure in the near-bottom water, especially under suboxic and anoxic conditions (Figs. 2–4). That means that the concentrations and fluxes change over every cm of the BBL and also temporally during the year. This should be taken into account while analyzing the data of observations and experiments, since the methods applied usually don't allow for fine-structure sampling. For example, in the standard methods of the sediment – water flux measurements with the box corers or benthic chambers, this fine structure is destroyed.

3.2 Comparison with data

Validation of the present complex multi-component model against data is not trivial, because it is hard to assemble a comprehensive dataset against which to calibrate the model components at a vertical resolution and temporal frequency that captures to the fine scale vertical structure and rapid temporal variation characteristic of the system. Even though such dataset is not yet assembled, we believe it is a worthy exercise to

GMDD
doi:10.5194/gmd-2015-239

present a model that captures a wide range of processes, thus providing a platform to test hypothesis and affine our conceptual understanding of anoxia.

Here we will provide relevant examples from regions with contrasting redox conditions where the model can be potentially use. Given that the water column model was parameterized for the Northern North Sea, we can compare our results against observations of the BBL under oxic conditions, collected recently in the Sleipner area (Linke et al., 2014; Queirós et al., 2014). Besides this, we can use the literature data on typical values or distributions collected in the other regions with suboxic and anoxic conditions.

For example the model is able to simulate the periodic succession of oxic, hypoxic and anoxic bottom waters following winter oxygenation that is documented for many years with very rare (4 times a year) observations for the Elefsis Bay in the Aegean Sea (Pavlidou et al., 2013).

The modelled concentrations and vertical distributions of dissolved oxygen, inorganic nitrogen species (nitrate, nitrite, ammonia), silicates, phosphates and iron and manganese species (Fe(II), Fe(III), Mn(II), Mn(III), and Mn(IV)) in the water column, BBL and porewater of upper sediment layer as well as range of its benthic fluxes values are in good agreements with the measured data (Table 5) (Pakhomova et al., 2007; Almroth et al., 2009; Queirós et al., 2014).

3.2.1 Dissolved oxygen

The model reproduces changes of oxygen concentrations at the sediment–water interface from 200 µM in oxygenated period to 0 µM during the anoxia. The field data in the Sleipner area show DO oscillations from 160 to 360 µM in the bottom water during observations taken over a two-month period (Linke et al., 2014). The modeled downward vertical flux of oxygen was found to the highest in the water column below the euphotic zone in winter and early spring, it and sporadically exceeds 200 $\mathrm{mmol\,m^{-2}\,d^{-1}}$, in connection with the mixing intensity changes (Figs. 6 and 7). In the limits of the BBL oxygen flux decreases from about 10 to 0 $\mathrm{mmol\,m^{-2}\,d^{-1}}$, corresponding to the typical values of the oxygen flux that can be received in the field and laboratory experiments.

GMDD
doi:10.5194/gmd-2015-239

For example, during the chamber experiments there was measured sediment oxygen consumption in the range 3.9–4.6 mmol m^{-2} d^{-1} in the Sleipner area (Queirós et al., 2014) and 5–13 mmol m^{-2} d^{-1} in the Gulf of Finland, Vistula Lagoon, and shelf Black Sea (Almroth et al., 2009; Pakhomova et al., 2007). While in organic rich sediments, oxygen flux could reach up to 70 mmol m^{-2} d^{-1} (Pakhomova et al., 2004, 2003).

The sediment pore water profile measured during the laboratory experiment shows oxygen depletion at 9 mm depth in oxic conditions and at 3 mm depth in hypoxic conditions (Queirós et al., 2014). That corresponds well with the modeled distribution of oxygen (Fig. 2).

Unfortunately, further observations under anoxic and suboxic conditions are rare, as field and experimental studies generally focus on oxic conditions. While the model can describe the biogeochemistry of the bottom areas with the restricted aeration, i.e. trenches and methane sips where hypoxia and anoxia can occur, lack of observations make it difficult to validate the corresponding model predictions, e.g., the disappearance of oxygen in the sediments, and in the near-bottom water during the stagnation period (Figs. 3 and 4).

3.2.2 Nitrogen

The modelled concentrations of nitrate in the water column correspond to the climatic values (Boyer et al., 2013). The flux of NO_3 changed its direction (Fig. 7). In oxic conditions an upward flux of nitrate exists in the limits of the BBL and in the water column, compensating the loss of nitrate for photosynthesis production. In suboxic conditions there is a downward flux of nitrate connected with denitrification. The modelled upward values of the nitrate flux in the BBL −0.5–2 mmol m^{-2} d^{-1} in oxic period are within the range of measured values (from −0.5 to 2.5 mmol m^{-2} d^{-1}) (Almroth et al., 2009; Queirós et al., 2014).

In the sediments the modelled nitrogen was represented by ammonia with concentrations 250 µM, that is 2 times higher than measured during the experiments for nonsulphydic sediments, 120 µM, (Queirós et al., 2014) but is typical for sulphidic sediments

GMDD
doi:10.5194/gmd-2015-239

(Almroth et al., 2009). The flux of ammonia is directed upward throughout the year, and changes from 0.03 mmol m^{-2} d^{-1} during the oxic period to more than 1 mmol m^{-2} d^{-1} during the anoxic period. The measured ammonia flux was in the range from −1 to 6 mmol m^{-2} d^{-1} (Almroth et al., 2009; Queirós et al., 2014) was highest for anoxic sediments.

3.2.3 Phosphorus

The modelled concentrations of phosphate increased from 0–2 µM in the the water column to around 4 µM in the BBL, which is higher than typical measured at oxic conditions values but could be found above the sulphidic sediments. Modelled phosphate concentrations in the upper sediments (up to 30–35 µM) were higher than the measured values of around 5 µM for nonsulphidic sediment (Queirós et al., 2014) but of the same level as for sulphidic sediment (15–50 µM, Almroth et al., 2009). Modelled phosphate fluxes in the BBL were less than 0.01 mmol m^{-2} d^{-1} in oxic conditions, increasing to 0.01 mmol m^{-2} d^{-1} in anoxic; these are comparable with measured values ranging from −1 to 0.9 mmol m^{-2} d^{-1} for oxic sediment (Queirós et al., 2014) but are lower than for sulphidic sediments (1.5 mmol m^{-2} d^{-1}, Almroth et al., 2009).

3.2.4 Manganese

Under oxic conditions the modelled manganese content was negligible in the water column and the sediment–water interface was characterized by an accumulation of Mn(IV). Beneath the maximum of Mn(IV) a peak of Mn(III) is formed, followed by a Mn(II) maximum and finally by a $MnCO_3$ and MnS increase, in agreement with the modern paradigm of Mn species distributions in the sediments (Madison et al., 2013). From qualitative point of view the modelled Mn(II) concentrations in the upper sediment (8–20 µM) were about the same level obtained for sulphidic sediments (5–30 µM in the coastal Black Sea, 25–50 µM in the Gulf of Finland, Pakhomova et al., 2007) and lower

GMDD
doi:10.5194/gmd-2015-239

than for nonsulphidic sediments (over 100 µM, Pakhomova et al., 2007; Queirós et al., 2014).

The model predicted the observed small concentrations of Mn(III) and Mn(II) in the bottom water during the stagnation period, but the modelled concentrations of Mn(II) were much smaller than observed. Modelled fluxes of Mn(IV), Mn(III) and Mn(II) were negligible (less than 0.1 mmol m^{-2} d^{-1}) while the measured fluxes varied from −3 to 20 mmol m^{-2} d^{-1} (Pakhomova et al., 2007; Queirós et al., 2014). To our knowledge, this is the first time that the distributions of Mn(III), a form of Mn that has only recently been considered (Madison et al., 2013), is included in a reaction network for sediment biogeochemistry.

The modelled concentration of Mn as solid $MnCO_3$ in upper sediment layers reached up to 11 µM that corresponds to 0.04 % of Mn in the sediment (using transformation coefficient between dissolved and solid phases, F = 0.66). The same average level of Mn is observed in sulphidic sediments 0.01–1 % (Calvert and Pedersen, 1993; Pakhomova et al., 2007). Simulated by the model negligible concentrations of MnS in upper sulphidic sediment were is in agreement with field observation in many regions.

3.2.5 Iron

The distributions and variability of iron species were similar to those of manganese. As for Mn(II) the maximum modelled concentrations of Fe(II) in pore water (8–40 µM) were smaller than measured for nonsulphidic sediments (over 100 µM) (Pakhomova et al., 2007; Queirós et al., 2014) but slightly higher level than for sulphidic sediments (0.5–7 µM, Pakhomova et al., 2007). Modelled fluxes of Fe(III) and Fe(II) (up to 0.1 mmol m^{-2} d^{-1}) were the same order of magnitude as average measured fluxes for sulphidic sediments, 0.04 and 0.3 mmol m^{-2} d^{-1} for Fe(III) and Fe(II) respectively. Both modelled and measured Fe(II) fluxes were highest at suboxic conditions in bottom water while measured Fe(II) fluxes could reach 1 mmol m^{-2} d^{-1} (Pakhomova et al., 2007).

GMDD
doi:10.5194/gmd-2015-239

3.3 Carbonate system

The modelled distributions of the carbonate system, their variability and fluxes are shown in Figs. 5–7.

In the upper water layer pH values are high (8.10 in winter and 8.23 in summer), the values of pCO_2 are close to the equilibrium with the atmosphere (about 400 ppm). Calcium carbonate is oversaturated (about 2.5 for aragonite and about 3.5 for calcite). The values of total alkalinity (2300 µM) and DIC (2200 µM) are close to the typical values for the open ocean.

In the seasonally anoxic deep water layer and the BBL pH oscillated from 7.6 in oxygenated period to 7.1 during anoxia. pCO_2 varies from to 1200–1500 ppm to 2500–2800 ppm. Aragonite and calcite saturations change from 0.6 and 1.0 in oxic conditions to 0.2 and 0.4 in anoxic conditions, respectively. Total alkalinity and DIC are lower under oxic conditions (2200–2300 and 2200 µM) and larger values during anoxic conditions (2400 and 2500 µM).

In the upper 12 cm of the sediment pH decreases from 7.1–7.4 to 6.6, and pCO_2 increases from 2500–4000 ppm to is about 17 000–23 000 ppm. The performed calculations show that, under natural conditions, there are significant season variations in the carbonate saturation and pH values in the BBL. Modelled $CaCO_3$ was present in small concentrations (0.5 µM) at the SWI only in the oxygenated period (Fig. 5).

It is known that the processes connected with changes of redox conditions represent an important factor of influence on the carbonate system and alkalinity. For example, pH dynamics caused by OM degradation are buffered by precipitation and dissolution of carbonates (Luff et al., 2001), sulphate reduction produces large amount of bicarbonate-ion (Boudreau, 1996), Mn reduction increases alkalinity by producing bicarbonate and consuming protons (Sternbeck, 1996), and Fe reduction leads to a consumption of protons (Luff et al., 2001).

The potential role of a such processes in the pH and alkalinity changes was analyzed by (Soetaert et al., 2007). In this model we simulate the combined effect of the

GMDD
doi:10.5194/gmd-2015-239

mentioned processes in a scenario of variations of the bottom redox conditions from oxic into anoxic.

The comparison between the main seawater alkalinity components shown in Table 6 demonstrates that even in the anoxic conditions the contributions of such components A_{TPO_4}, A_{Si}, A_{TNH_3}, A_{TH_2S} remain small compared with the carbonate alkalinity. The modeled mechanism of significant alkalinity changes is connected with redox processes (listed in Sect. 2.1.1) that produce or remove H^+ or OH^- and the redox processes connected with OM mineralization (i.e. sulphate reduction, Mn reduction and Fe reduction). Because the protolithic reactions are very fast the results of these processes reflects in the ratio between carbonate and bicarbonate in a larger degree than in production/consumption of the forms of alkalinity that increases in anoxic conditions (i.e. A_{TPO_4}, A_{Si}, A_{TNH_3}, A_{TH_2S}).

According to the model, at the sediment surface this resulted in a decrease of pH from 7.6 in oxic period to 7.1 in anoxic (Fig. 5). In the sediments, pH decreased with depth to 6.6–6.7 at 12 cm. During the stagnation period, a pH minimum could be marked out at 1 cm depth where there was also a maximum of H_2S (Fig. 4) and maximum of pCO_2, A_T and DIC. All this hints at a dominant role for sulfate reduction, which particularly affects the ratio between DIC and A_T that determines pH (i.e. analyzed by Luff et al., 2001). The upper sediment alkalinity maximum during the anoxic period subsequently smoothes and propagates into the deeper layers, leading to lower alkalinity during the oxic period. At the boundary between the BBL and the water column the alkalinity flux changes its direction from downward in oxic conditions to upward in anoxic conditions. At the SWI the alkalinity flux is directed upward with much smaller values in oxic than in anoxic conditions (Fig. 7).

The bottom water is close to saturation regarding calcite and undersaturation regarding aragonite during the oxygenated period, and is undersaturated regarding both calcite and aragonite during the anoxic period. Deeper in the sediment aragonite (to a larger degree) and calcite (to a smaller degree) are always undersaturated. Note that

GMDD
doi:10.5194/gmd-2015-239

according to the model assumption the sediment carbonate system processes were forced by the upper boundary.

The model calculations clearly demonstrates the impact of redox conditions on the carbonate system and alkalinity and consequently, their role in regulating carbon transformation and transport.

3.4 Modeling analyses of the role of chemosynthesis and bioturbation

The model allows a quantitative analysis of how the processes interact and combine. It is possible to "unlock" or accelerate certain processes and to demonstrate their specific significance. Here we demonstrate this possibility on assessing of a role of chemosynthesis and bioturbation in the bottom biogeochemistry.

For baseline simulations, we assumed the following parameters values: $k_{Baan\_gro} = 0.012\,d^{-1}$ for anaerobic autotrophs chemosynthesis specific growth rate, and $K_{z\_bio\_max} = 1 \times 10^{-11}\,m^2\,s^{-1}$ for maximum bioturbation/bioirrigation coefficient.

To assess an effect of chemosynthesis and bioturbation on the distribution of the model variables was calculated with varying k_{Baan_gro}: (a) $k_{Baan\_gro} = 0.012\,d^{-1}$ (baseline) and (b) $k_{Baan\_gro} = 0.060\,d^{-1}$ and $K_{z\_bio\_max}$: (i) $K_{z\_bio\_max} = 0\,m^2\,s^{-1}$, (ii) $K_{z\_bio\_max} = 1 \times 10^{-11}\,m^2\,s^{-1}$ (baseline) and $K_{z\_bio\_max} = 10 \times 10^{-11}\,m^2\,s^{-1}$. The results are shown in Fig. 8.

The model experiment showed that bioturbation affects the depth of oxygen penetrations. In case of an absence of bioturbation that is less than 1 mm (ai), in case of a baseline bioturbation it is 2–4 mm (aii). In case of an increased bioturbation (aiii), oxygen penetration increases to 8–10 mm in the sediment column (Fig. 8). In this case, the model predicts a pH minimum at the vicinity of depth of oxygen penetration. This is consistent with oxygen consuming reactions by reduced forms of S, N, Mn, Fe which consumes proton.

An increase of the chemosynthesis rate (Fig. 8, column b) leads to a formation of a pH maximum just below the SWI that is connected with the consumption of CO_2,

GMDD
doi:10.5194/gmd-2015-239

affecting the ratio between DIC and A_T. This maximum is more pronounced in the absence of bioturbation (bi) and is not pronounced under high bioturbation (biii). This pH maximum produces a maximum in calcite saturation, which could favor the organisms with carbonate skeletons.

The pH distributions with a maximum below the SWI is usually explained by an electron transfer by long filamentous bacteria or grain to grain contacts between conductive materials (Meysman et al., 2015; Nielsen et al., 2010), but this model shows that chemosynthesis can have a similar effect.

4 Summary and conclusion

This paper presents a coupled benthic-pelagic model that reproduces different redox conditions and their impact on the distributions of a wide range of biogeochemical variables.

The comparison with the available data allows us to conclude that the model reproduces distributions and fluxes of key biogeochemical variables during the periodic change of redox conditions. That allows us to conclude the following:

- The main driver of the redox state at the SWI is the formation of anoxia in the water column. That arises by an imbalance between the supply of OM and dissolved oxygen to the bottom water, which in turn is due to seasonality in production and consumption of OM, as well as mixing.
- The model captures the time lag between disappearance of dissolved oxygen and appearance of H_2S in the bottom water. That is connected with Mn and Fe oxides, which buffer the H_2S efflux from the sediments after complete oxygen consumption. These oxides acts as “batteries”, that are using up in anoxic periods and accumulates during oxic periods.
- The model also demonstrates that redox conditions have a pronounced impact on the carbonate system and on alkalinity, which in turn affects carbon transforma-

GMDD
doi:10.5194/gmd-2015-239

tion and transport. It is shown that in anoxic conditions the total alkalinity changes in a larger degree because of variation of the ratio between carbonate and bicarbonate due to fast redox reactions producing or consuming proton, than because of and an increase or decrease of other alkalinity components (i.e. A_{TPO_4}, A_{Si}, A_{TNH_3}, A_{TH_2S}).

– Bacteria play a significant role in the fate of OM due to chemosynthesis (autotrophs) and consumption of DOM (heterotrophs). In particular, in certain conditions, the consumption of CO_2 in chemosynthesis can lead to the formation of a pH maximum below the SWI.

In summary, the capability of BROM to reproduce seasonal variations in oxygen concentration and redox state, to resolve fine scale structure of the water column, BBL and sediment and to capture the time lags associated with rarely modelled compounds (e.g., Mn and Fe oxides role in securing of the H_2S efflux, pH, alkalinity, carbonate saturation change) presents a wide range of possibilities for use in applications.

Code availability

The BROM model source code is publicly available as part of the official FABM distribution at http://fabm.net. Being a part of FABM, BROM uses modern software standards: it is coded in object-oriented Fortran 2003, has a build system based on CMake, and uses YAML files for configuration.

Author contributions. Development of the model code was made by E. Yakushev, E. Protsenko, J. Bruggeman, S. Yakubov, analyses of the model results and discussions were conducted by R. Bellerby, R. Couture and S. Pakhomova, all authors contributed to the writing of the manuscript.

Acknowledgements. We acknowledge funding from the EC 7th Framework Program (FP7/2007–2013) under grant agreement no 265 847 ("Sub-seabed CO2 Storage: Impact on Marine Ecosystems", ECO2) and 240 837 ("Research into Impacts and Safety in CO2

GMDD
doi:10.5194/gmd-2015-239

Storage", RISCS), with additional development funds from FME SUCCESS, CO2Base, EEA CO2MARINE, Norwegian Research Council project no. 236 658 ("New knowledge on sea deposits" NYKOS), the Research Council of Norway through its Centers of Excellence funding scheme, project number 223 268/F50 (CERAD), contract no. 208 279 (NIVA Strategic Institute Initiative "Climate effects from Mountains to Fjords"), NIVA OASIS, and VISTA – a basic research program and collaborative partnership between the Norwegian Academy of Science and Letters and Statoil, project no. 6164.

References

Almroth, E., Tengberg, A., Andersson, J. H., Pakhomova, S., and Hall, P. O. J.: Effects of resuspension on benthic fluxes of oxygen, nutrients, dissolved inorganic carbon, iron and manganese in the Gulf of Finland, Baltic Sea, Cont. Shelf Res., 29, 807–818, doi:10.1016/j.csr.2008.12.011, 2009.

Anderson, J. J., Okubo, A., Robbins, A. S., and Richards, F. A.: A model for nitrite and nitrate distributions in oceanic oxygen minumum zones, Deep-Sea Res., 29, 1113–1140, 1982.

Bektursunova, R. and L'Heureux, I.: A reaction-transport model of periodic precipitation of pyrite in anoxic marine sediments, Chem. Geol., 287, 158–170, 2011.

Blackwelder, P., Hood, T., Alvarez-Zarikian, C., Nelsen, T. A., and McKee, B.: Benthic foraminifera from the necop study area impacted by the Mississippi River plume and seasonal hypoxia, Quatern. Int., 31, 19–36, doi:10.1016/1040-6182(95)00018-E, 1996.

Bolding, K., Burchard, H., Pohlmann, T., and Stips, A.: Turbulent mixing in the northern North Sea: a numerical model study, Cont. Shelf Res., 22, 2707–2724, 2002.

Boudreau, B. P.: A method-of-lines code for carbon and nutrient diagenesis in aquatic sediments, Comput. Geosci., 22, 479–496, doi:10.1016/0098-3004(95)00115-8, 1996.

Boudreau, B. P.: Diagenetic Models and Their Impletation: Modelling Transport and Reactions in Aquatic Sediments, Springer-Verlag, Berlin, Heidelberg, NY, 414 pp., 1997.

Boyer, T. P., Antonov, J. I., Baranova, O. K., Coleman, C., Garcia, H. E., Grodsky, A., Johnson, D. R., Locarnini, R. A., Mishonov, A. V., O'Brien, T. D., Paver, C. R., Reagan, J. R., Seidov, D., Smolyar, I. V., and Zweng, M. M.: World Ocean Database 2013, NOAA Atlas NESDIS 72, edited by: Levitus, S. and Mishonov, A., Silver Spring, MD, USA, 209 pp., doi:10.7289/V5NZ85MT, 2013.

GMDD

doi:10.5194/gmd-2015-239

Bruggeman, J. and Bolding, K.: A general framework for aquatic biogeochemical models, Environ. Modell. Softw., 61, 249–265, doi:10.1016/j.envsoft.2014.04.002, 2014.
Calvert, S. E. and Pedersen, T. F.: Geochemistry of Recent oxic and anoxic marine sediments: implications for the geological record, Mar. Geol., 113, 67–88, 1993.
Canfield, D. E., Kristensen, E., and Thamdrup, B.: Aquatic geomicrobiology, Adv. Mar. Biol., 48, 1–599, doi:10.1016/S0065-2881(05)48011-6, 2005.
Cooper, D. C. and Morse, J. W.: The chemistry of Offatts Bayou, Texas: a seasonally highly sulfidic basin, Estuaries, 19, 595–611, doi:10.2307/1352520, 1996.
Davison, W.: Iron and manganese in lakes, Earth-Sci. Rev. 34, 119–163, 1993.
Debolskaya, E. I., Yakushev, E. V., and Kuznetsov, I. S.: Analysis of the hydrophysical structure of the Sea of Azov in the period of the bottom anoxia development, J. Marine Syst., 70, 300–307, doi:10.1016/j.jmarsys.2007.02.027, 2008.
Diaz, R. J. and Rosenberg, R.: Spreading dead zones and consequences for marine ecosystems, Science, 321, 926–929, doi:10.1126/science.1156401, 2008.
Dickson, A. G.: The development of the alkalinity concept in marine chemistry, Mar. Chem., 40, 49–63, doi:10.1016/0304-4203(92)90047-E, 1992.
Glud, R. N.: Oxygen dynamics of marine sediments, Mar. Biol. Res., 4, 243–289, doi:10.1080/17451000801888726, 2008.
He, Y., Stanev, E. V., Yakushev, E., and Staneva, J.: Black Sea biogeochemistry: response to decadal atmospheric variability during 1960–2000 inferred from numerical modeling, Mar. Environ. Res., 77, 90–102, doi:10.1016/j.marenvres.2012.02.007, 2012.
Jorgensen, B., Bang, M., and Blackburn, T.: Anaerobic mineralization in marine sediments from the Baltic Sea-North Sea transition, Mar. Ecol.-Prog. Ser., 59, 39–54, doi:10.3354/meps059039, 1990.
Jourabchi, P., Meile, C., Pasion, L. R., and Van Cappellen, P.: Quantitative interpretation of pore water O_2 and pH distributions in deep-sea sediments, Geochim. Cosmochim. Ac., 72, 1350–1364, doi:10.1016/j.gca.2007.12.012, 2008.
Kamyshny, A., Yakushev, E., Jost, G., and Podymov, O.: Chemical Structure of Pelagic Redox Interfaces, The Handbook of Environmental Chemistry, edited by: Yakushev, E., Springer, Berlin, Heidelberg, Germany, 2013.
Kappler, A., Emerson, D., Edwards, K., Amend, J. P., Gralnick, J. A., Grathwohl, P., Hoehler, T., and Straub, K. L.: Microbial activity in biogeochemical gradients – new aspects of research, Geobiology, 3, 229–233, doi:10.1111/j.1472-4669.2005.00053.x, 2005.

GMDD
doi:10.5194/gmd-2015-239

Katsev, S. and Dittrich, M.: Modeling of decadal scale phosphorus retention in lake sediment under varying redox conditions, Ecol. Model., 251, 246–259, doi:10.1016/j.ecolmodel.2012.12.008, 2013.

Katsev, S., Chaillou, G., Sundby, B., and Mucci, A.: Effects of progressive oxygen depletion on sediment diagenesis and fluxes: a model for the lower St. Lawrence River Estuary, Limnol. Oceanogr., 52, 2555–2568, doi:10.4319/lo.2007.52.6.2555, 2007.

Lewis, E. and Wallace, D.: Program developed for CO_2 system calculations, ORNL/CDIAC-105. Carbon Dioxide Information Analysis Center, Oak Ridge National Laboratory, U.S. Department of Energy, Oak Ridge, Tennessee, USA, 1–21, 1998.

Linke, P., Haeckel, M., von Deimling, J. S., Vielstädte, L., Schmidt, M., Karstens, J., Berndt, C., Herreilers, H., Lichtschlag, A., James, R., Connelly, D., Baumberger, T., Pedersen, R. B., Denny, A. R., Rapp, H. T., Thorseth, I. H., Molari, M., de Beer, D., Rehder, G., Kedzior, S., Beaubien, S., and de Vittor, C.: Fluxes of CO_2 from Natural Seep Sites and Sleipner Storage Site, ECO2 Project Office, Kiel, Germany, available at: http://oceanrep.geomar.de/26057/ (last access: 20 December 2015), 2014.

Luff, R., Haeckel, M., and Wallmann, K.: Robust and fast FORTRAN and MATLAB libraries to calculate pH distributions in marine systems, Comput. Geosci., 27, 157–169, doi:10.1016/S0098-3004(00)00097-2, 2001.

Madison, A. S., Tebo, B. M., Mucci, A., Sundby, B., and Luther, G. W.: Abundant porewater Mn(III) is a major component of the sedimentary redox system, Science, 341, 875–878, doi:10.1126/science.1241396, 2013.

McCarthy, M. J., McNeal, K. S., Morse, J. W., and Gardner, W. S.: Bottom-water hypoxia effects on sediment–water interface nitrogen transformations in a seasonally hypoxic, shallow bay (Corpus Christi Bay, TX, USA), Estuar. Coast., 31, 521–531, doi:10.1007/s12237-008-9041-z, 2008.

Meysman, F. J., Risgaard-Petersen, N., Malkin, S. Y., and Nielsen, L. P.: The geochemical fingerprint of microbial long-distance electron transport in the seafloor, Geochim. Cosmochim. Ac., 152, 122–142, 2015.

Millero, F. J.: Thermodynamics of the carbon dioxide system in the oceans, Geochim. Cosmochim. Ac., 59, 661–677, doi:10.1016/0016-7037(94)00354-O, 1995.

Morgan, J. J.: Manganese speciation and redox kinetics in natural waters, Environm. Engn., 3, 475–478, 2000.

GMDD

doi:10.5194/gmd-2015-239

Bottom RedOx Model (BROM, v.1.0)

E. V. Yakushev et al.

Morse, J. W. and Eldridge, P. M.: A non-steady state diagenetic model for changes in sediment biogeochemistry in response to seasonally hypoxic/anoxic conditions in the “dead zone” of the Louisiana shelf, Mar. Chem., 106, 239–255, doi:10.1016/j.marchem.2006.02.003, 2007.

Nielsen, L. P., Risgaard-Petersen, N., Fossing, H., Christensen, P. B., and Sayama, M.: Electric currents couple spatially separated biogeochemical processes in marine sediment, Nature, 463, 1071–1074, doi:10.1038/nature08790, 2010.

Pakhomova, S. V., Kononets, M. Y., Yudin, M. V., and Rozanov, A. G.: Studies on the fluxes of dissolved forms of iron and manganese through the water–bottom interface on the north-eastern shelf of the Black Sea, Oceanology, 43, 493–497, 2003.

Pakhomova, S. V., Kononets, M. Y., Yudin, M. V., Vershinin, A. V., and Rozanov, A. G.: Studies on the fluxes of dissolved metal forms through the water–bottom interface in vistula lagoon of the Baltic sea, Oceanology, 44, 481–488, 2004.

Pakhomova, S. V., Hall, P. O. J., Kononets, M. Y., Rozanov, A. G., Tengberg, A., and Vershinin, A. V.: Fluxes of iron and manganese across the sediment–water interface under various redox conditions, Mar. Chem., 107, 319–331, doi:10.1016/j.marchem.2007.06.001, 2007.

Paraska, D. W., Hipsey, M. R., and Salmon, S. U.: Sediment diagenesis models: review of approaches, challenges and opportunities, Environ. Modell. Softw., 61, 297–325, doi:10.1016/j.envsoft.2014.05.011, 2014.

Pavlidou, A., Kontoyiannis, H., Anagnostou, C., Siokou–Frangou, I., Pagou, K., Krasakopoulou, E., Assimakopoulou, G., Zervoudaki, S., Zeri, C., Chatzianestis, J., and Psyllidou-Giouranovits, R.: Biogeochemical characteristics in the Elefsis Bay (Aegean Sea, eastern Mediterranean) in relation to anoxia and climate changes, in: The Handbook of Environmental Chemistry, edited by: Yakushev, E., NIVA, Springer, Berlin, Heidelberg, Germany, 161–201, 2013.

Queirós, A. M., Norling, K., Amaro, T., Nunes, J., Cummings, D., Yakushev, E., Sorensen, K., Harris, C., Woodward, M., Danovaro, R., Rastelli, E., Alve, E., Vittor, C. De, Karuza, A., Cibic, T., Monti, M., Ingrosso, G., Fornasaro, D., Beaubien, S. E., Guilini, K., Vanreu, A., Bigalke, N., and Widdicombe, S.: Potential impact of CCS leakage on marine communities, ECO2 Deliverable, D4.1, Plymouth Marine Laboratory, 86 pp., doi:10.3289/ECO2_D4.1, 2014.

GMDD

doi:10.5194/gmd-2015-239

Rabalais, N. N., Turner, R. E., and Scavia, D.: Beyond science into policy: Gulf of Mexico hypoxia and the Mississippi River, Bioscience, 52, 129–142, doi:10.1641/0006-3568(2002)052[0129:BSIPGO]2.0.CO;2, 2002.

Richards, F.: Anoxic basins and fjords, in: Chemical Oceanography, edited by: Riley, J. and Skirrow, G., Academic Press, London, UK, 611–645, 1965.

Richardson, K. and Jørgensen, B..: Eutrophication: Definition, History and Effects, in: Eutrophication in Coastal Marine Systems. Coastal and Estuarine Studies 52, edited by: Jørgensen, B. B. and Richardson, K., AGU, Washington, DC, USA, 1–19, 1996.

Roden, E. E. and Tuttle, J. H.: Sulfide release from estuarine sediments underlying anoxic bottom water, Limnol. Oceanogr., 37, 725–738, doi:10.4319/lo.1992.37.4.0725, 1992.

Roy, R. N., Roy, L. N., Vogel, K. M., Porter-Moore, C., Pearson, T., Good, C. E., Millero, F. J., and Campbell, D. M.: The dissociation constants of carbonic acid in seawater at salinities 5 to 45 and temperatures 0 to 45 °C, Mar. Chem., 44, 249–267, doi:10.1016/0304-4203(93)90207-5, 1993.

Schippers, A. and Jorgensen, B. B.: Biogeochemistry of pyrite and iron sulfsulphide oxidation in marine sediments, Geochim. Cosmochim, Ac„ 66, 85–92, 2002.

Sell, K. S. and Morse, J. W.: Dissolved Fe_2^+ and $\sum H_2S$ behavior in sediments seasonally overlain by hypoxic-to-anoxic waters as determined by CSV Microelectrodes, Aquat. Geochem., 12, 179–198, doi:10.1007/s10498-005-4574-2, 2006.

Sen Gupta, B. K., Turner, R. E., and Rabalais, N. N.: Seasonal oxygen depletion in continental-shelf waters of Louisiana: historical record of benthic foraminifers, Geology, 24, 227–230, doi:10.1130/0091-7613(1996)024<0227:SODICS>2.3.CO;2, 1996.

Soetaert, K., Hofmann, A. F., Middelburg, J. J., Meysman, F. J. R., and Greenwood, J.: The effect of biogeochemical processes on pH (reprinted from Mar. Chem., 105, 30–51, 2007), Mar. Chem., 106, 380–401, doi:10.1016/j.marchem.2007.06.008, 2007.

Stanev, E. V., He, Y., Staneva, J., and Yakushev, E.: Mixing in the Black Sea detected from the temporal and spatial variability of oxygen and sulfide – Argo float observations and numerical modelling, Biogeosciences, 11, 5707–5732, doi:10.5194/bg-11-5707-2014, 2014.

Sternbeck, J.: Manganese cycling in a eutrophic lake – rates and pathways, Aquat. Geochem., 1, 399–426, doi:10.1007/BF00702741, 1996.

Tebo, B. M., Ghiorse, W. C., van Waasbergen, V. G., Siering, P. L., and Caspi, L.: Bacterially mediated mineral foundation: Insights into manganese (II) oxidation from molecular genetic and biochemical studies, in: Reviews in Mineralogy, edited by: Banfield, J. F. and Nealson,

GMDD

doi:10.5194/gmd-2015-239

K. H., Vol. 35, Geomicrobiology Interactions berween Microbs and Minerals. Mineralogical Society of America, Washington, DC, USA, 225–266, 1997.
Van Cappellen, P. and Wang, Y. F.: Cycling of iron and manganese in surface sediments: A general theory for the coupled transport and reaction of carbon, oxygen, nitrogen, sulfur, iron, and manganese, Am. J. Sci., 296, 197–243, 1996.
Vershinin, A. V. and Rozanov, A. G.: Chemical Exchange across the Sediment – Water Interface in Oceans and Seas, GEOS, Moscow, Russia, 164 pp., 2002.
Volkov, I. I.: Geokhimiya Sery v Osadkakh Okeana (Geochemistry of Sulfur in Ocean Sediments), Nauka, Moscow, Russia, 1984.
Wanninkhof, R.: Relationship between wind speed and gas exchange over the ocean revisited, Limnol. Oceanogr., 12, 351–362, doi:10.4319/lom.2014.12.351, 2014.
Wijsman, J. W. M., Herman, P. M. J., Middelburg, J. J., and Soetaert, K.: A model for early diagenetic processes in sediments of the continental shelf of the Black Sea. Estuarine, Coastal and Shelf Science, 54, 403–421, 2002.
Wolf-Gladrow, D. A., Zeebe, R. E., Klaas, C., Körtzinger, A., and Dickson, A. G.: Total alkalinity: the explicit conservative expression and its application to biogeochemical processes, Mar. Chem., 106, 287–300, doi:10.1016/j.marchem.2007.01.006, 2007.
Yakushev, E. V.: RedOx layer model: a tool for analysis of the water column oxic/anoxic interface processes, in: Chemical Structure of Pelagic Redox Interfaces: Observation and Modeling, Hdb. Env. Chem. (2013) 22, edited by: Yakushev, E. V., Springer-Verlag, Berlin, Heidelberg, Germany, 203–234, 2013.
Yakushev, E. and Debolskaya, E.: Particulate manganese as a main factor of oxidation of hydrogen sulfide in redox zone of the Black Sea, in: Konstantin Fedorov Memorial Symposium, Oceanic Fronts and Related Phenomena, Saint-Petersburg, Russia, 18–22 May 1998, Proceedings. IOC Workshop Report No. 159, Kluwer Academic Publishers, 592–597, 2000.
Yakushev, E. V., Pollehne, F., Jost, G., Kuznetsov, I., Schneider, B., and Umlauf, L.: Redox Layer Model (ROLM): a Tool for Analysis of the Water Column Oxic/anoxic Interface Processes, Meereswissenschaftliche Berichte, Marine Scince Report, vol. 68, Instutut fur Ostseeforschung Warnemuende, 54 pp., 2006.
Yakushev, E., Pakhomova, S., Sørenson, K., and Skei, J.: Importance of the different manganese species in the formation of water column redox zones: observations and modeling, Mar. Chem., 117, 59–70, doi:10.1016/j.marchem.2009.09.007, 2009.

GMDD
doi:10.5194/gmd-2015-239

Yakushev, E. V., Pollehne, F., Jost, G., Kuznetsov, I., Schneider, B., and Umlauf, L.: Analysis of the water column oxic/anoxic interface in the Black and Baltic seas with a numerical model, Mar. Chem., 107, 388–410, doi:10.1016/j.marchem.2007.06.003, 2007.

Yakushev, E. V., Kuznetsov, I. S., Podymov, O. I., Burchard, H., Neumann, T., and Pollehne, F.: Modeling the influence of oxygenated inflows on the biogeochemical structure of the Gotland Sea, central Baltic Sea: changes in the distribution of manganese, Comput. Geosci., 37, 398–409, doi:10.1016/j.cageo.2011.01.001, 2011.

Yu, L., Fennel, K., Laurent, A., Murrell, M. C., and Lehrter, J. C.: Numerical analysis of the primary processes controlling oxygen dynamics on the Louisiana shelf, Biogeosciences, 12, 2063–2076, doi:10.5194/bg-12-2063-2015, 2015.

Zeebe, R. E. and Wolf-Gladrow, D.: CO_2 in Seawater: Equilibrium, Kinetics, Isotopes, Elsevier Oceanography Series 65, Amsterdam, the Netherlands, 2001.

GMDD

doi:10.5194/gmd-2015-239

Table 1. State variables of BROM. Concentrations are presented in micromoles for chemical variables and in micromoles of nitrogen for biological variables.

Notation	Name	Units
O – oxygen		
O_2	dissolved oxygen	µM O
S – sulfur		
H_2S	hydrogen sulfide	µM S
S^0	total elemental sulfur	µM S
S_2O_3	thiosulfate and sulfites	µM S
SO_4	sulfate	µM S
N – nitrogen		
NH_4	ammonia	µM N
NO_2	nitrite	µM N
NO_3	nitrate	µM N
PON	particulate organic nitrogen	µM N
DON	dissolved organic nitrogen	µM N
P – phosphorus		
PO_4	phosphate	µM P
Si – silicate		
Si	dissolved silicon	µM Si
Si_part	particulate silicon	µM Si
Mn – manganese		
MnII	dissolved bivalent manganese	µM Mn
MnIII	dissolved trivalent manganese	µM Mn
MnIV	particulate quadrivalent manganese	µM Mn
MnS	manganese sulfide	µM Mn
$MnCO_3$	manganese carbonate	µM Mn
Fe – iron		
FeII	dissolved bivalent iron	µM Fe
FeIII	particulate trivalent iron	µM Fe
FeS	iron sulfide	µM Fe
FeS_2	iron pyrite	µM Fe
C – carbon		
DIC	dissolved inorganic carbon	µM C
Ca – calcium		
$CaCO_3$	Calcium carbonate	µM Ca
Alkalinity		
Alk	total alkalinity	µM
Biological parameters		
Phy	phototrophic producers	µM N
Het	pelagic and benthic heterotrophs	µM N
Bhae	aerobic heterotrophic bacteria	µM N
Baae	aerobic autotrophic bacteria	µM N
Bhan	anaerobic heterotrophic bacteria	µM N
Baan	anaerobic autotrophic bacteria	µM N

GMDD
doi:10.5194/gmd-2015-239

Table 2. Parameterization of the biogeochemical processes.

Name of Process, reference, reaction	Parameterization in the model
Autolysis Mineralization at oxic conditions (Richards, 1965) $(CH_2O)_{106}(NH_3)16H_3PO_4 + 106O_2 \rightarrow 106CO_2 + 16NH_3 + H_3PO_4 + 106H_2O$	Autolysis N = $K_{PON\_DON} \times$ PON DcDM_O_2 = $K_{DON\_ox} \times$ DON $\times$ Fox $\times (1 + f_t^D(t))$ DcPM_O_2 = $K_{PON\_ox} \times$ PON $\times$ Fox $\times (1 + f_t^D(t))$ where Fox = $\frac{O_2}{O_2 + K_{omoxO_2}}$; $f_t^D(t) = B_{da}\frac{t^2}{t^2 + t_{da}^2}$
Manganese	
Manganese(II) oxidation (Canfield et al., 2005) $4Mn^{2+} + O_2 + 4H^+ \rightarrow 4Mn^{3+} + 2H_2O$	mn_ox = $0.5 \times \left(1 + \tanh\left(Mn^{2+} - s_{mnox_{mn2}}\right)\right) \times K_{mn\_ox} \times Mn^{2+} \times \frac{O_2}{(O_2 + k_{mnoxO_2})}$
Manganese (III) oxidation (Tebo et al., 1997) $2Mn^{3+} + 3H_2O + 0.5O_2 \rightarrow 2MnO_2 + 6H^+$	mn_ox2 = $0.5 \times \left(1 + \tanh\left(Mn^{3+} - s_{mnox_{mn3}}\right)\right) \times K_{mn_{ox2}} \times Mn^{3+} \times \frac{O_2}{(O_2 + k_{mnoxO_2})}$
Manganese (IV) reduction $2MnO_2 + 7H^+ + HS^- \rightarrow 2Mn^{3+} + 4H_2O + S^0$	mn_rd = $0.5 \times \left(1 + \tanh\left(Mn^{4+} - s_{mnrd_{mn4}}\right)\right) \times K_{mn_{rd}} \times Mn^{4+} \times \frac{H_2S}{(H_2S + k_{mnrdHS})}$
Manganese (III) reduction $2Mn^{3+} + HS^- \rightarrow 2Mn^{2+} + S^0 + H^+$	mn_rd2 = $0.5 \times \left(1 + \tanh\left(Mn^{3+} - s_{mnrd_{mn3}}\right)\right) \times K_{mn_{rd2}} \times Mn^{3+} \times \frac{H_2S}{(H_2S + k_{mnrdHS})}$
MnS formation/dissollution (Davison, 1993) $Mn^{2+} + HS^- \leftrightarrow MnS + H^+$	mns_prec = $K_{mns_{form}} \times \max\{0, (om\_mns - 1)\}$ mns_diss = $K_{mns_{diss}} \times$ MnS $\times \max\{0, (1 - om\_mns)\}$ where om_mns = $\frac{H_2S \times Mn^{2+}}{K_{mns} \times H^+}$
$MnCO_3$ precipitation/dissolution (Van Capellen, Wang, 1996) $Mn^{2+} + CO_3^- \leftrightarrow MnCO_3$	mnco3_prec = $K_{mnco3_{form}} \times \max\{0, (om\_mnco3 - 1)\}$ mnco3_diss = $K_{mnco3_{diss}} \times MnCO_3 \times \max\{0, (1 - om_{mnco_3})\}$ where $om_{mnco_3} = \frac{Mn^{2+} \times CO_3}{K_{mnco_3}}$
$MnCO_3$ oxidation by O_2 (Morgan, 2005) $2MnCO_3 + O_2 + 2H_2O = 2MnO_2 + 2HCO_3^- + 2H^+$	mn_co3_ox = $K_{mnco3_{ox}} \times MnCO_3 \times O_2$
Manganese reduction for PON (Boudreau, 1996) $(CH_2O)_{106}(NH_3)_{16}H_3PO_4 + 212MnO_2 + 318CO_2 + 106H_2O \rightarrow 424HCO_3^- + 212Mn^{2+} + 16NH_3 + H_3PO_4$	DcPM_Mn = $\max\left\{0, K_{PON_{Mn}} \times PON \times \frac{Mn^{4+}}{Mn^{4+}+0.5}\right\} \times (1 - 0.5 \times (1 + \tanh(O_2 - O_2 s_{dn})))$
Manganese reduction for DON (Boudreau, 1996)	DcDM_Mn = $\max\left\{0, K_{DON_{Mn}} \times DON \times \frac{Mn^{4+}}{Mn^{4+}+0.5}\right\} \times (1 - 0.5 \times (1 + \tanh(O_2 - O_2 s_{dn})))$

GMDD
doi:10.5194/gmd-2015-239

Table 2. Continued.

Name of Process, reference, reaction	Parameterization in the model
Iron	
Fe (II) oxidation with O_2 (Van Cappelen, Wang, 1996) $4Fe^{2+} + O_2 + 10H_2O \rightarrow 4Fe(OH)_3 + 8H^+$	$fe\_ox = 0.5 \times \left(1 + \tanh\left(Fe^{2+} - s^{2+}_{feox_{fe}}\right)\right) \times K_{fe_{ox}} \times O_2 \times Fe^{2+}$
Fe (II) oxidation with Mn oxide (Van Cappelen, Wang, 1996) $2Fe^{2+} + MnO_2 + 4H_2O \rightarrow 2Fe(OH)_3 + Mn^{2+} + 2H^+$	$fe\_ox2 = 0.5 \times \left(1 + \tanh\left(Fe^{2+} - s_{feox_{Fe^{2+}}}\right)\right) \times K_{fe_{ox}} \times Mn^{4+} \times Fe^{2+}$
Fe (III) reduction (Volkov, 1984) $2Fe(OH)_3 + HS^- + 5H^+ \rightarrow 2Fe^{2+} + S^0 + 6H_2O$	$fe\_rd = 0.5 \times \left(1 + \tanh\left(Fe^{3+} - s_{ferd_{Fe^{3+}}}\right)\right) \times K_{fe_{rd}} \times Fe^{3+} \times \frac{H_2S}{H_2S + K_{ferd} HS}$
FeS formation/dissolition (Bektursunova et al., 2011) $Fe^{2+} + HS^- \leftrightarrow FeS + H^+$	$fes\_form = K_{FeS_{form}} \max\{0, (om_{FeS} - 1)\}$ $fes\_diss = K_{FeS_{diss}} \max\{0, (1 - om_{fe})\}$ where $om_{FeS} = \frac{H_2S \times Fe^{2+}}{K_{FeS} \times H^+}$
FeS oxidation (Soetaert et al., 2007) $FeS + 2.25O_2 + 2.5H_2O \rightarrow Fe(OH)_3 + 2H^+ + SO_4^{2-}$	$fes\_ox = K_{FeS_{ox}} \times O_2 \times FeS$
Pyrite formation (Rickard, 1997; Soetaert et al., 2007) $FeS + H_2S \rightarrow FeS_2 + H_2$	$fes2\_form = K_{FeS_{2form}} \times H_2S \times FeS$
Pyrite oxidation by O_2 (Wijsman et al., 2002) $FeS_2 + 3.5O_2 + H_2O \rightarrow Fe^{2+} + 2SO_4^{2-} + 2H^+$	$fes2\_ox = K_{FeS_{2ox}} \times FeS_2 \times O_2$
Iron reduction for DON (Boudreau, 1996) $(CH_2O)_{106}(NH_3)_{16}H_3PO_4 + 424Fe(OH)_3 + 742CO_2 \rightarrow 848HCO_3^- + 424Fe^{2+} + 318H_2O + 16NH_3 + H_3PO_4$	$DcDM\_Fe = K_{DON_{Fe}} \times DON \times Fe^{3+} \times \left(1. - 0.5 \times \left(1 + \tanh\left(O_2 - O_{2s_{dn}}\right)\right)\right)$
Iron reduction for PON (Boudreau, 1996)	$DcPM\_Fe = K_{PON_{Fe}} \times PON \times Fe^{3+} \times \left(1. - 0.5 \times \left(1 + \tanh\left(O_2 - O_{2s_{dn}}\right)\right)\right)$

GMDD
doi:10.5194/gmd-2015-239

Table 2. Continued.

Name of Process, reference, reaction	Parameterization in the model
Nitrogen	
Nitrification 1 stage (Canfield et al., 2005) $NH_4^+ + 1.5O_2 \rightarrow NO_2^- + 2H^+ + H_2O$	nitrif1 = $K_{N42} \times NH_4 \times O_2 \times 0.5 \times (1 + \tanh(O_2 - O_2\_s\_nf))$
Nitrification 2 stage (Canfield et al., 2005) $NO_2^- + 0.5O_2 \rightarrow NO_3^-$	nitrif2 = $K_{N23} \times NO_2 \times O_2 \times 0.5 \times \left(1 + \tanh\left(O_2 - O_{2s_{nf}}\right)\right)$
Anammox (Canfield et al., 2005) $NO_2^- + NH_4^+ \rightarrow N_2 + 2H_2O$	anammox = $K_{anammox} \times NO_2 \times NH_4 \times \left(1 - 0.5 \times \left(1 + \tanh\left(O_2 - O_{2s_{dn}}\right)\right)\right)$
POM and DOM denitrification (1st stage) (Anderson et al., 1982) $0.5CH_2O + NO_3^- \rightarrow NO_2^- + 0.5H_2O + 0.5CO_2$	denitr1_PM = $K_{N32} \times PON \times Fdnox \frac{NO_3}{NO_3 + K_{omno_{NO_3}}}$ denitr1_DM = $K_{N32} \times DON \times Fdnox \times \frac{NO_3}{NO_3 + K_{omno_{NO_3}}}$ denitr1 = denitr1_PM + denitr1_DM where Fdnox = $\left(1 - 0.5 \times \left(1 + \tanh\left(O_2 - O_{2S_{dn}}\right)\right)\right)$
POM and DOM denitrification (2d stage) (Anderson et al., 1982) $0.75CH_2O + H^+ + NO_2^- \rightarrow 0.5N_2 + 1.25H_2O + 0.75CO_2$	denitr2_PM = $K_{N24} \times PON \times Fdonx \times \frac{NO_2}{NO_2 + K_{omno\_NO2}}$ denitr2_DM = $K_{N24} \times DON \times Fdnox \times \frac{NO_2}{NO_2 + K_{omno\_NO2}}$ denitr2 = denitr2_PM + denitr2_DM
Denitrification of POM and DOM (Richards, 1965) $(CH_2O)_{106}(NH_3)_{16}H_3PO_4 + 84.8HNO_3 = 106CO_2 + 42.4N_2 + 148.4H_2O + 16NH_3 + H_3PO_4$	DcPM_NOX = $\frac{16}{212} \times$ Denitr1_PM + $\frac{16}{141.3}$Denitr2_PM DcDM_NOX = $\frac{16}{212} \times$ Denitr1_DM + $\frac{16}{141.3}$Denitr2_DM

GMDD
doi:10.5194/gmd-2015-239

Table 2. Continued.

Name of Process, reference, reaction	Parameterization in the model
Sulfur	
S^0 disproportionation (Canfield et al., 2005) $4S^0 + 3H_2O \rightarrow 2H_2S + S_2O_3^{2-} + 2H^+$	disprop = $K_{dispro} \times S^0$
Sulphide oxidation with O_2 (Volkov, 1984) $2H_2S + O_2 \rightarrow 2S^0 + 2H_2O$	hs_ox = $K_{HS_{ox}} \times H_2S \times O_2$
S^0 oxidation with O_2 (Volkov, 1984) $2S^0 + O_2 + H_2O \rightarrow S_2O_3^{2-} + 2H^+$	s0_ox = $K_{S^0\_ox} \times S^0 \times O_2$
S^0 oxidation with NO_3 (Kamyshny et al., 2013) $4S^0 + 3NO_3^- + 7H_2O \rightarrow 4SO_4^{2-} + 3NH_4^+ + 2H^+$	s0_no3 = $K^0_{S_{NO_3}} \times NO_3 \times S^0$
S_2O_3 oxidation with O_2 (Volkov, 1984) $S_2O_3^{2-} + 2O_2 + 2OH^- \rightarrow 2SO_4^{2-} + H_2O$	s2o3_ox = $K_{s23\_ox} \times S_2O_3 \times O_2$
S_2O_3 oxidation with NO_3 (Kamyshny et al., 2013) $S_2O_3^{2-} + NO_3^- + 2H_2O \rightarrow 2SO_4^{2-} + NH_4^+$	s2o3_no3 = $K_{S23\_NO_3} \times NO_3 \times S_2O_3$
Thiodenitrification (Volkov, 1984; Schippers and Jorgensen, 2002) $5H_2S + 8NO_3^- + 2OH^- \rightarrow 5SO_4^{2-} + 4N_2 + 6H_2O$	sulfido = $KT \times H_2S \times NO_3$
POM sulfatereduction 1st and 2d stages (Boudreau, 1996) $(CH_2O)_{106}(NH_3)_{16}H_3PO_4 + 53SO_4^{2-} \rightarrow 106HCO_3^- + 16NH_3 + H_3PO_4 + 53H_2S$	s4rd_PM = $K_{s4_{rd}} \times$ Fsox $\times$ Fsnx $\times SO_4 \times$ PON s23rd_PM = $K_{s23_{rd}} \times$ Fsox $\times$ Fsnx $\times S_2O_3 \times$ PON where: Fsox = $(1. - 0.5 \times (1. + \tanh(O_2 - s_{omso_{o2}})))$ Fsnx = $(1. - 0.5 \times (1. + \tanh(NO_3 - s_{omso_{no}})))$ DcPM_SO_4 = $16/53 \times (s4_{rd_{PM}} + s23_{rd_{PM}})$
DOM sulfatereduction 1st and 2d stages (Boudreau, 1996):	s4rd_DM = $K_{s4_{rd}} \times$ Fsox $\times$ Fsnx $\times SO_4 \times$ DON s23rd_DM = $K_{s23_{rd}} \times$ Fsox $\times$ Fsnx $\times S_2O_3 \times$ DON DcDM_SO_4 = $16/53 \times (s4_{rd_{DM}} + s23_{rd_{DM}})$

GMDD
doi:10.5194/gmd-2015-239

Table 2. Continued.

Name of Process, reference, reaction	Parameterization in the model
Carbon and Alkalinity	
Carbonate system	Carbonate system equilibration was parameterized using the standard approach (i.e. Lewis and Wallace, 1998)
$CaCO_3$ precipitation/dissolution (Luff et al., 2001) $Ca^{2+} + CO_3^{2} \leftrightarrow CaCO_3$	caco3_prec = $K_{CaCO_{3prec}} \times \max\{0, (om\_CaCO_3 - 1)\}$ caco3_diss = $K_{CaCO_{3diss}} \times CaCO_3 \times \max\{0, (1 - om\_CaCO_3)\}^{4.5}$ $om\_CaCO_3 = \frac{Ca^{2+} \times CO_3}{K_{CaCO_3}}$
Alkalinity changes	In addition to the standard Alkalinity components (i.e. Dickson, 1992), there were parameterized changes due to consumption or producing of a proton (see the text for details) in biogeochemical reactions and the nutrient-H+-compensation principle for OM production and decay (Wolf-Gladrow et al., 2007) dAlk = $-Nitrif1 + (Denitr2\_PM + Denitr2\_DM) + 2 \times (s4\_rd + s23\_rd) + mn\_ox - 3 \times mn\_ox2 + 3 \times mn\_rd - mn\_rd2 - 2 \times mns\_prec + 2 \times mns\_diss - 2 \times mnco3\_prec + 2 \times mnco3\_diss + 26.5 \times (DcDM\_Mn + DcPM\_Mn) - 2 \times fe\_ox - fe\_ox2 + 2 \times fe\_rd - fes\_prec + fes\_diss - 2 \times fes\_ox - 2 \times fes2\_ox + 53 \times (DcDM\_Fe + DcPM\_Fe) - 0.5 \times Disprop + s0\_ox - 0.5 \times s0\_no3 - s23\_ox - 0.4 \times sulfido - 2 \times CaCO_3\_prec + 2 \times CaCO_3$
Silicate	
Dissolution of particulate Si (Popova, Srokosz, 2009)	sipart_diss = $Si_{part} \times K_{si_{part_{diss}}}$

GMDD
doi:10.5194/gmd-2015-239

Table 2. Continued.

Name of Process, reference, reaction	Parameterization in the model
Phytoplankton	
Irradiance changing with depth	$Iz = Io \times e^{(-k_{Erlov} \times z)} \times e^{(-kc \times turbid \times 0.0001)}$
Influence of the irradiance on photosynthesis	$LimLight = (Iz/Iopt) \times e^{(1-Iz/Iopt)}$
Influence of temperature on photosynthesis	$LimT = e^{(bm \times t\text{-}cm)}$
Dependence of photosynthesis on P	$LimP = \frac{(PO_4/Phy)^2}{(KPO_4 \times NkP)^2 + (PO_4/Phy)^2}$
Dependence of photosynthesis on NO_3	$LimNH_3 = \frac{(NH_3/Phy)^2}{KNH_3^2 + (NH_3/Phy)}^2$
Dependence of photosynthesis on NH_4	$LimNH_4 = \frac{(NH_4/Phy)^2}{KNH_4^2 + (NH_4/Phy)}^2$
Influence of N on photosynthesis	$LimN = LimNO_3 + LimNH_4$
Growth of phytoplankton	$GrowthPhy = KNF \times LimLight \times LimT \times \min(LimP, LimN) \times Phy$
Excretion rate phyto	$ExcrPhy = K_{FD} \times Phy$
Phy mortality rate	$MortPhy = (KFP + 0.45 \times (0.5 - 0.5 \times \tanh(O_2 - 60)) + 0.45 \times (0.5 - 0.5 \times \tanh(O_2 - 20))) \times Phy$

GMDD
doi:10.5194/gmd-2015-239

Table 2. Continued.

Name of Process, reference, reaction	Parameterization in the model
Heterotrophs	
Grazing of Het	Grazing = GrazPhy + GrazPOP + GrazBact
Grazing of Het on Phy	$\text{GrazPhy} = \text{KFZ} \times \text{Het} \times \frac{(\text{Phy}/(\text{Het}+0.0001))^2}{K_{FY}^2+(\text{Phy}/(\text{Het}+0.0001))^2}$
Grazing of Het on detritus	$\text{GrazPOP} = \text{KPZ} \times \text{Het} \times \frac{\left(\frac{\text{PON}}{\text{Het}+0.0001}\right)^2}{(\text{KPP})^2+\left(\frac{\text{PON}}{\text{Het}+0.0001}\right)^2}$
Grazing of Het on bacteria	GrazBact = GrazBaae + GrazBaan + GrazBhae + GrazBhan
Grazing of Het on bacteria autotrophic aerobic	$\text{GrazBaae} = \text{KPZ} \times \text{Het} \times \frac{(\text{Baae}/(\text{Het}+0.0001))^2}{\text{limGrazBac}^2+(\text{Baae}/(\text{Het}+0.0001))^2}$
Grazing of Het on bacteria autotrophic anaerobic	$\text{GrazBaan} = 0.5 \times \text{KPZ} \times \text{Het} \times \frac{(\text{Baan}/(\text{Het}+0.0001))^2}{\text{limGrazBac}^2+(\text{Baan}/(\text{Het}+0.0001))^2}$
Grazing of Het on bacteria heterotrophic aerobic	$\text{GrazBhae} = \text{KPZ} \times \text{Het} \times \frac{(\text{Bhae}/(\text{Het}+0.0001))^2}{\text{limGrazBac}^2+(\text{Bhae}/(\text{Het}+0.0001))^2}$
Grazing of Het on bacteria heterotrophic anaerobic	$\text{GrazBhan} = 1.3 \times \text{KPZ} \times \text{Het} \times \frac{(\text{Bhan}/\text{Het}+0.0001)^2}{\text{limGrazBac}^2+(\text{Bhan}/\text{Het}+0.0001)^2}$
Respiration rate of Het	$\text{RespHet} = \text{KZN} \times \text{Het} \times (0.5 + 0.5 \times \tanh(O_2 - 20))$
Mortality of Het	$\text{MortHet} = \text{Het} \times (0.25 + 0.3 \times (0.5 - 0.5 \times \tanh(O_2 - 20)) + 0.45 \times (0.5 + 0.4 \times \tanh(H_2S - 10)))$

GMDD
doi:10.5194/gmd-2015-239

Table 2. Continued.

Name of Process, reference, reaction	Parameterization in the model
Bacteria	
Growth rate of Bacteria aerobic autotrophic	$\text{ChemBaae} = (\text{Nitrif1} + \text{Nitrif2} + \text{mn}_{ox} + \text{fe}_{ox} + \text{s23}_{ox} + \text{s0}_{ox} + \text{anammox}) \times \text{k\_Baae\_gro} \times \text{Baae} \times \min\left(\frac{(\text{NH}_4/(\text{Baae}+0.0001))^2}{\text{limBaae}^2+(\text{NH}_4/(\text{Baae}+0.0001))^2}, \frac{(\text{PO}_4/(\text{Baae}+0.0001))^2}{\text{limBaae}^2+(\text{PO}_4/(\text{Baae}+0.0001))^2}\right)$
Rate of mortality of Bacteria aerobic autotrophic	$\text{MortBaae} = K_{\text{Baae}_{mrt}} + K_{\text{Baae}_{mrt_{h2s}}} \times 0.5 \times (1 - \tanh(1 - \text{H}_2\text{S})) \times \text{Baae}^2$
Growth rate of Bacteria aerobic heterotrophic	$\text{HetBhae} = \left(\text{DcPM}_{\text{O}_2} + \text{DcDM}_{\text{O}_2}\right) \times \text{K\_Bhae}_{gro} \times \text{Bhae} \times \frac{(\text{DON}/(\text{Bhae}+0.0001))^2}{\text{limBhae}^2+(\text{DON}/(\text{Bhae}+0.0001))^2}$
Rate of mortality of Bacteria aerobic heterotrophic	$\text{MortBhae} = \text{K}_{\text{Bhae}_{mrt}} + \text{K}_{\text{Bhae}_{mrt_{h2s}}} \times \text{Bhae} \times 0.5 \times (1 - \tanh(1 - \text{H}_2\text{S}))$
Growth rate of Bacteria anaerobic autotrophic	$\text{ChemBaan} = (\text{mn}_{rd} + \text{mn}_{rd2} + \text{fe}_{rd} + \text{hs}_{ox} + \text{sulfido}) \times \text{K\_Baan}_{gro} \times \text{Baan} \times \min\left(\frac{(\text{NH}_4/(\text{Baan}+0.0001))^2}{\text{limBaan}^2+(\text{NH}_4/(\text{Baan}+0.0001))^2}\right)$
Rate of mortality of Bacteria anaerobic autotrophic	$\text{MortBaan} = \text{k\_Baan}_{mrt} \times \text{Baan}$
Growth rate of Bacteria anaerobic heterotrophic	$\text{HetBhan} = (\text{DcPM}_{\text{NOX}} + \text{DcDM}_{\text{NOX}} + \text{DcPM}_{\text{SO}_4} + \text{DcDM}_{\text{SO}_4} + \text{DcPM}_{\text{Mn}}\text{DcDm}_{\text{Mn}} + \text{DcPM}_{\text{Fe}} + \text{DcDM}_{\text{Fe}}) \times \text{K\_Bhan}_{gro} \times \text{Bhan} \times \frac{(\text{DON}/(\text{Bhan}+0.0001))^2}{\text{limBhan}^2+(\text{DON}/(\text{Bhan}+0.0001))^2}$
Rate of mortality of Bacteria anaerobic heterotrophic	$\text{MortBhan} = \text{k}_{\text{Bhan}_{mrt}} + \text{K}_{\text{Bhan}_{mrt_{\text{O}_2}}} \times \text{Bhan} \times (0.5 + 0.5 \times \tanh(1 - \text{O}_2))$
Summarized OM mineralization	$\text{Dc}_{\text{OM}_{total}} = \text{DcDM}_{\text{O}_2} + \text{DcPM}_{\text{O}_2} + \text{DcPM}_{\text{NOX}} + \text{DcDM}_{\text{NOX}} + \text{DcDM}_{\text{Mn}} + \text{DcPM}_{\text{Mn}} + \text{DcDM}_{\text{Fe}} + \text{DcPM}_{\text{Fe}} + \text{DcDM}_{\text{SO}_4} + \text{DcDM}_{\text{SO}_4}$

GMDD
doi:10.5194/gmd-2015-239

Table 3. Parameters names, notations, values and units of the coefficients used in the model.

Parameter	Notation	Units	Value
Manganese			
Specific rate of Mn(II) to Mn(III) oxidation with O_2	K_mn_ox	d^{-1}	0.1
Specific rate of Mn(IV) to Mn(III) reduction with H_2S	K_mn_rd	d^{-1}	0.5
Specific rate of Mn(III) to Mn(IV) oxidation with O_2	K_mn_ox2	d^{-1}	0.2
Specific rate of Mn(III) to Mn(II) reduction with H_2S	K_mn_rd2	d^{-1}	1.0
Specific rate of formation of MnS from Mn(II) and H_2S	K_mns_form	d^{-1}	1×10^{-5}
Specific rate of dissolution of MnS to Mn(II) and H_2S	K_mns_diss	d^{-1}	5×10^{-4}
Conditional equilibrium constant for MnS	K_mns	M	1500
Conditional equilibrium constant for $MnCO_3$	K_mnco3	M	15
Specific rate of $MnCO_3$ dissolution	K_mnco3_diss	d^{-1}	7×10^{-4}
Specific rate of $MnCO_3$ formation	K_mnco3_form	d^{-1}	3×10^{-4}
Specific rate of DON Oxidation with Mn(IV)	K_DON_Mn	d^{-1}	1×10^{-3}
Specific rate of PON Oxidation with Mn(IV)	K_PON_Mn	d^{-1}	1×10^{-3}
Threshold value of Mn(II) oxidation	s_mnox_mn2	µM Mn	0.01
Threshold value of Mn(III) oxidation	s_mnox_mn3	µM Mn	0.01
Threshold value of Mn(IV) reduction	s_mnrd_mn4	µM Mn	0.01
Threshold value of Mn(III) reduction	s_mnrd_mn3	µM Mn	0.01

GMDD
doi:10.5194/gmd-2015-239

Table 3. Continued.

Parameter	Notation	Units	Value
Iron			
Specific rate of Fe(II) to Fe(III) oxidation with O_2	K_{fe_ox}	d^{-1}	0.5
Specific rate of Fe(II) to Fe(III) oxidation with MnO_2	K_{fe_ox2}	d^{-1}	1×10^{-3}
Specific rate of Fe(III) to Fe(II) reduction with H_2S	K_{fe_rd}	d^{-1}	0.5
Conditional equilibrium constant for FeS	K_{FeS}	µM	2510
Specific rate of FeS formation from Fe(II) and H_2S	K_{Fes_form}	d^{-1}	5×10^{-4}
Specific rate of DON oxidation with Fe(III)	K_{DON_Fe}	d^{-1}	5×10^{-5}
Specific rate of PON oxidation with Fe(III)	K_{PON_Fe}	d^{-1}	1×10^{-5}
Specific rate of FeS_2 formation by reaction of FeS with H_2S	K_{FeS2_form}	d^{-1}	1×10^{-6}
Specific rate of FeS_2 oxidation with O_2	K_{FeS2_ox}	d^{-1}	4.4×10^{-4}
Threshold value of Fe(II) reduction	s_{feox_fe2}	µM Fe	1×10^{-3}
Threshold value of Fe(III) reduction	s_{ferd_fe3}	µM Fe	0.01
Sulfur			
Specific rate of H_2S oxidation to S^0 of with O_2	K_{hs_ox}	d^{-1}	0.5
Specific rate of S^0 oxidation of with O_2	K_{s0_ox}	d^{-1}	0.02
Specific rate of S^0 oxidation of with NO_3	$K_{S0\_NO_3}$	d^{-1}	0.9
Specific rate of S_2O_3 oxidation with O_2	K_{s23_ox}	d^{-1}	0.01
Specific rate of S_2O_3 oxidation with NO_3	$K_{s23\_NO_3}$	d^{-1}	0.01
Specific rate of Sulfate reduction with sulfate	K_{s4_rd}	d^{-1}	5×10^{-6}
Specific rate of sulfate reduction with thiosulfate	K_{s23_rd}	d^{-1}	1×10^{-3}
Specific rate of S^0 disproportionation	K_{dispro}	d^{-1}	1×10^{-3}

GMDD
doi:10.5194/gmd-2015-239

Table 3. Continued.

Parameter	Notation	Units	Value
Nitrogen			
Specific rate of DON oxidation of with O_2	$K_{\_DON\_ox}$	d^{-1}	0.01
Specific rate of PON oxidation of with O_2	$K_{\_PON\_ox}$	d^{-1}	2×10^{-3}
Temperature control threshold coefficient for OM decay	Tda	°C	13
Temperature control coefficient for OM decay	beta_da	–	20
Half-saturation constant of O_2 for OM mineralization	$K_{\_omox\_o2}$	µM	1
Specific rate of decomposition of PON to DON	$K_{\_PON\_DON}$	d^{-1}	0.1
Strength of ammonium inhibition of nitrate uptake constant	K_{psi}	–	1.46
Half saturation constant for uptake of NO_3+NO_2	K_{NO_3}	µM	0.15
Half saturation constant for uptake of NH_4	K_{NH_4}	µM	0.02
Specific rate of the 1st stage of nitrification	K_{N42}	d^{-1}	0.01
Specific rate of the 2d stage of nitrification	K_{N23}	d^{-1}	0.1
Specific rate of 1st stage of denitrification	K_{N32}	d^{-1}	0.16
Specific rate of 2d stage of denitrification	K_{N24}	d^{-1}	0.25
Half-saturation of NO_2 for OM denitrification	k_omno_no3	µM N	1×10^{-3}
Half-saturation of NO_2 for OM denitrification	k_omno_no2	µM N	1×10^{-3}
Specific rate of thiodenitrification	K_T	d^{-1}	0.8
Specific rate of anammox	$K_{annamox}$	d^{-1}	0.8
Phosphorus			
Half-saturation constant for uptake of PO_4 by phytoplankton	K_{PO_4}	µM	0.02
Fe/P ratio in during co-precipitation with Fe oxides	r_fe_p		2.7
Mn/P ratio in complexes with Mn(III)	r_mn_p		0.67

GMDD
doi:10.5194/gmd-2015-239

Table 3. Continued.

Parameter	Notation	Units	Value
Oxygen			
Half-saturation constant for nitrification	O_{2s_nf}	µM	4.488
Half-saturation constant for denitrification	O_{2s_dn}	µM	10
Threshold value of O_2 for OM mineralization	s_omox_o2	µM	0.01
Threshold value of O_2 for OM denitrification	s_omno_o2	µM	25
Threshold value of O_2 for OM sulfate reduction	s_omso_o2	µM	25
Threshold value of NO for OM sulfate reduction	s_omso_no	µM	5
Half saturation constant of Mn oxidation	k_mnoxO2	µM O	2
Calcium			
Specific rate of $CaCO_3$ dissolution	K_CaCO3_diss	d^{-1}	3
Specific rate of $CaCO_3$ precipitation	K_CaCO3_prec	d^{-1}	1×10^{-4}
Silicon			
Specific rate of Si dissolution	K_Sipart_diss	d^{-1}	8×10^{-3}
Bacteria			
Baae maximum specific growth rate	k_Baae_gro	d^{-1}	0.008
Baae specific rate of mortality	k_Baae_mrt	d^{-1}	0.01
Baae increased specific rate of mortality due to H_2S	$k\_Baae\_mrt\_h2s$	d^{-1}	0.899
Bhae maximum specific growth rate	k_Bhae_gro	d^{-1}	0.5
Bhae specific rate of mortality	k_Bhae_mrt	d^{-1}	25×10^{-4}
Bhae increased specific rate of mortality due to H_2S	$k\_Bhae\_mrt\_h2s$	d^{-1}	0.799
Baan maximum specific growth rate	k_Baan_gro	d^{-1}	0.020
Baan specific rate of mortality	k_Baan_mrt	d^{-1}	5×10^{-3}
Bhan maximum specific growth rate	k_Bhan_gro	d^{-1}	0.1
Bhan specific rate of mortality	k_Bhan_mrt	d^{-1}	5×10^{-3}
Bhan increased specific rate of mortality due to O_2	$k\_Bhan\_mrt\_o2$	d^{-1}	0.899

GMDD
doi:10.5194/gmd-2015-239

Table 3. Continued.

Parameter	Notation	Units	Value
Phytoplankton			
Maximum specific growth rate	K_{NF}	d^{-1}	2.6
Extinction coefficient	K_Erlov	m^{-1}	0.05
Surface irradiance	I_0	$W\,m^{-2}$	80
Optimal irradiance	I_{opt}	$W\,m^{-2}$	25
1st coefficient for growth dependence on t	bm	$°C^{-1}$	0.12
2d coefficient for growth dependence on t	cm	–	1.4
Attenuation constant for the self-shading effect	Kc	$m^2\,mmol\,N^{-1}$	0.03
Specific respiration rate	K_{FN}	d^{-1}	0.05
Specific rate of mortality	K_{FP}	d^{-1}	0.10
Specific rate of excretion	K_{FD}	d^{-1}	0.05
Heterotrophs			
Maximum specific rate of grazing of Het on Phy	K_{FZ}	d^{-1}	1.0
Half-saturation constant for the grazing of Het on Phy for Phy / Het ratio	K_{FY}	–	1.1
Maximum specific rate of grazing of Het on POP	K_{PZ}	d^{-1}	0.7
Specific respiration rate	K_{ZN}	d^{-1}	0.02
Half-saturation constant for the grazing of Het on POP in dependence to ratio POP/Het	K_{PP}	–	0.2
Maximum specific rate of mortality of Het	K_{ZP}	d^{-1}	0.05
Food absorbency for Heterotrophs	U_z	–	0.5
Ratio between dissolved and particulate excretes of Heterotrophs	H_z	–	0.5
Limiting parameter for bacteria grazing by Het	limGrazBac	–	2
Limiting parameter for bacteria anaerobic heterotrophic	limBhan	–	2
Limiting parameter for bacteria aerobic heterotrophic	limBhae	–	5
Limiting parameter for bacteria anaerobic autotrophic	limBaan	–	2
Limiting parameter for bacteria aerobic autotrophic	limBaae	–	1

GMDD
doi:10.5194/gmd-2015-239

Table 3. Continued.

Parameter	Notation	Units	Value
Sinking			
Rate of sinking of Phy	W_{Phy}	$m\,d^{-1}$	0.1
Rate of sinking of Het	W_{Het}	$m\,d^{-1}$	1.0
Rate of sinking of bacteria (Bhe, Bae, Bha, Baa)	W_{Bact}	$m\,d^{-1}$	0.4
Rate of sinking of detritus (POP, PON)	W_{sed}	$m\,d^{-1}$	5
Rate of accelerated sinking of particles with settled Mn hydroxides	W_{M}	$m\,d^{-1}$	7

GMDD
doi:10.5194/gmd-2015-239

Table 4. Rates of biogeochemical production/consumption of the model compartments.

Oxygen (O_2)	R_{O2} = (GrowthPhy – DcDM_O2 – DcPM_O2 – RespHet)OkN – 0.5mn_ox – 0.25mn_ox2 – 0.25fe_ox – 2mns_ox – 2fes_ox – 0.5hs_ox – 0.5s0_ox – s23_ox – 1.5Nitrif1 – 0.5Nitrif2 – (DcDM_O2 – DcPM_O2 + GrowthPhy – RespHet)OkN
Phosphate (PO_4)	R_{PO_4} = (DcDM_O2 + DcPM_O2 + DcPM_NOX + DcDM_NOX + DcDM_SO_4 + DcPM_SO_4 + DcDM_Mn + DcPM_Mn + DcDM_Fe + DcPM_Fe – Chemos – ChemosA – GrowthPhy + RespHet)/NkP – (fe_ox + fe_ox2)/2.7 – (mn_ox + mn_rd)/0.67 + fe_rd/2.7 + (mn_ox2 + mn_rd2)/0.67
Particulate Organic Nitrogen (PON)	R_{PON} = –autolis – DcPM_O2 – DcPM_NOX – DcPM_SO_4 – DcPM_Mn – DcPM_Fe + MortBaut + MortBautA + MortBhet + MortBhetA + MortPhy + MortHet + Grazing × (1 – Uz) × (1 – Hz) – GrazPOP
Dissolved Organic Phosphorus (DON)	R_{DON} = autolis – DcDM_O2 – DcDM_NOX – DcDM_ – DcDM_Mn – DcDM_Fe – Hetero – HeteroA + ExcrPhy + Grazing × (1 – Uz) × Hz
Ammonia (NH_4)	R_{NH_4} = DcDM_O2 + DcPM_O2 + DcPM_NOX + DcDM_NOX + DcDM_Mn + DcPM_Mn + DcDM_Fe + DcPM_Fe + DcDM_SO_4 + DcPM_SO_4 – Nitrif1 – anammox + RespHet – GrowthPhy × (LimNH4/LimN) – Chemos – ChemosA
Nitrite (NO_2)	R_{NO_2} = Nitrif1 – Nitrif2 + Denitr1 – Denitr2 – anammox – GrowthPhy × (LimNO3/LimN)(NO2/(NO2 + NO3))
Nitrate (NO_3)	R_{NO_3} = Nitrif2 – Denitr1 – sulphido × 1.25 – GrowthPhy × (LimNO3/LimN)(NO3/(NO2 + NO3))
Hydrogen sulphide (H_2S)	R_{H_2S} = –0.5mn_rd – 0.5mn_rd2 – 0.5fe_rd – hs_ox – fes_form – mns_form + 0.5Disprop – sulphido + s23_rd
Elemental sulphur (S^0)	RS0 = hs_ox + 0.5mn_rd + 0.5mn_rd2 + 0.5fe_rd – s0_ox – Disprop – S_{0_NO3}
Thiosulphate (S_2O_3)	R_{S2O3} = 0.5s0_ox – 0.5s23_ox + 0.25Disprop + 0.5s4_rd – 0.5s23_rd – S_{23_NO3}
Sulphate (SO_4)	R_{SO_4} = sulphido – s4_rd + s23_ox + fes_ox + mns_ox
Bivalent manganese (Mn(II))	R_{Mn2} = –mn_ox + mn_rd2 – mns_form + mns_ox + fe_ox2 + 2DcDM_Mn + 2DcPM_Mn
Quadrivalent manganese (Mn(IV))	R_{Mn4} = mn_ox2 – mn_rd – fe_ox2 – 2DcDM_Mn – 2DcPM_Mn
Trivalent manganese (Mn(III))	R_{Mn3} = mn_ox – mn_ox2 + mn_rd – mn_rd2
Manganese sulphide (MnS)	R_{MnS} = mns_form – mns_ox
Bivalent iron (Fe(II))	R_{Fe2} = –fe_ox – fe_ox2 + fe_rd – fes_form + fes_ox + 4DcDM_Fe + 4DcPM_Fe
Trivalent iron (Fe(III))	R_{Fe3} = fe_ox + fe_ox2 – fe_rd – 4DcDM_Fe – 4DcPM_Fe
Iron sulphide (FeS)	R_{FeS} = fes_form – fes_ox
Dissolved Inorganic Carbon (DIC)	R_{DIC} = (DcDM_O2 + DcPM_O2 + DcPM_NOX + DcDM_NOX + DcDM_SO4 + DcPM_SO4 + DcDM_Mn + DcPM_Mn + DcDM_Fe + DcPM_Fe – Chemos – ChemosA – GrowthPhy + RespHet)CkN
Total alkalinity (Alk)	R_{Alk} = dAlk
Phytoplankton (Phy)	R_{Phy} = GrowthPhy(1 – K_{FN}) – MortPhy – ExcrPhy – GrasPhy
Heterotrophs (Het)	R_{Het} = Grazing × U_z – MortHet – K_{ZN} × Het
Aerobic heterotrophic bacteria (Bhe)	R_{Bhe} = C_{Bhe} – $Mort_{Bhe}$ – $Graz_{Bhe}$
Aerobic autotrophic bacteria (Bae)	R_{Bae} = C_{Bae} – $Mort_{Bae}$ – $Graz_{Bae}$
Anaerobic heterotrophic bacteria (Bha)	R_{Bha} = C_{Bha} – $Mort_{Bha}$ – $Graz_{Bha}$
Anaerobic autotrophic bacteria (Baa)	R_{Baa} = C_{Baa} – $Mort_{Baa}$ – $Graz_{Baa}$

GMDD
doi:10.5194/gmd-2015-239

Bottom RedOx Model (BROM, v.1.0)

E. V. Yakushev et al.

Table 5. Modelled and observed* ranges of porewater concentration of studied components and its benthic fluxes.

	water column concentration, µM		porewater concentration, µM		benthic flux, mmol m^{-2} d^{-1}	
	modelled	observed	modelled	observed	modelled	observed
O_2	0–320	0–360			−0 to −10	−4 to −13
NO_3	0–26	0–10	0–2	0–1	−0.5–2	−0.5–2.5
NO_2	0–0.3	0–1	0–4.5	0–2.8	−0.1–0.1	–
NH_4	0.1–16	0–25	80–300	50–300	0.03–1	−1–6
PO_4	0–4	0–6	5–50	5–100	0.01–0.2	−1–1.5
Si	0–300	1–150	200–1400	100–600	0.5–15	1.7–11
pH	7.0–8.3	6.9–8.4	6.6–7.3	7.1–7.9		
DIC	–	–	–	–	1–20	5 –50
Alk	2200–2300	2000–3300	3000–4900	2000–20 000	1– 5	3–200
MnII	0–1.5	0–12	8–20	5–200	0.01–0.1	−3–20
FeII	0–1.5	0–1.6	8–40	0.5–100	0.01–0.1	0.03–1

* Pakhomova et al. (2007); Almroth et al. (2011); Queirós et al. (2014).

GMDD
doi:10.5194/gmd-2015-239

Table 6. Typical concentrations (ranges of concentrations) of alkalinity in the seawater (in μM).

		Value, μM, in oxic(/anoxic) conditions	Source
A_{TCO_2}	$[HCO_3^-] + 2[CO_3^{2-}]$	2306	Typical seawater (Millero, 1979)
A_B	$[B(OH)_4^-]$	100	Typical seawater (Millero, 2008; Dickson, 2012)
A_{DOM}	DOC (15 % of total)	6–75	Sea water (Canfield et al., 2005; Kepkay, 2000)
A_{TH_2S}	$[HS^-]$	< 0/50	Black Sea (Volkov et al., 2000)
A_{Si}	$[SiO(OH)_3^-]$	< 10/40	Black Sea (Volkov et al., 2000)
A_{TPO_4}	$[HPO_4^{2-}] + 2[PO_4^{2-}] - [H_3PO_4]$	2/7	Black Sea (Volkov et al., 2000)
A_{TNH_3}	$[NH_3]$	< 2/5	Black Sea (Volkov et al., 2000)
A_{THF}	[HF] (total F)	68	Typical seawater (Millero, 2008; Dickson, 2012)
$[OH^-]$	$[OH^-]$	8	Typical seawater (Millero, 2008; Dickson, 2012)
$[H^+]$	$[H^+]$ (pH = 8.151 NBS)	0.007	Typical seawater (Millero, 1979)
A_{TSO_4}	$[HSO_4-]$	0.0015–0.010	Typical seawater (Hoffmann et al., 2008)

GMDD
doi:10.5194/gmd-2015-239

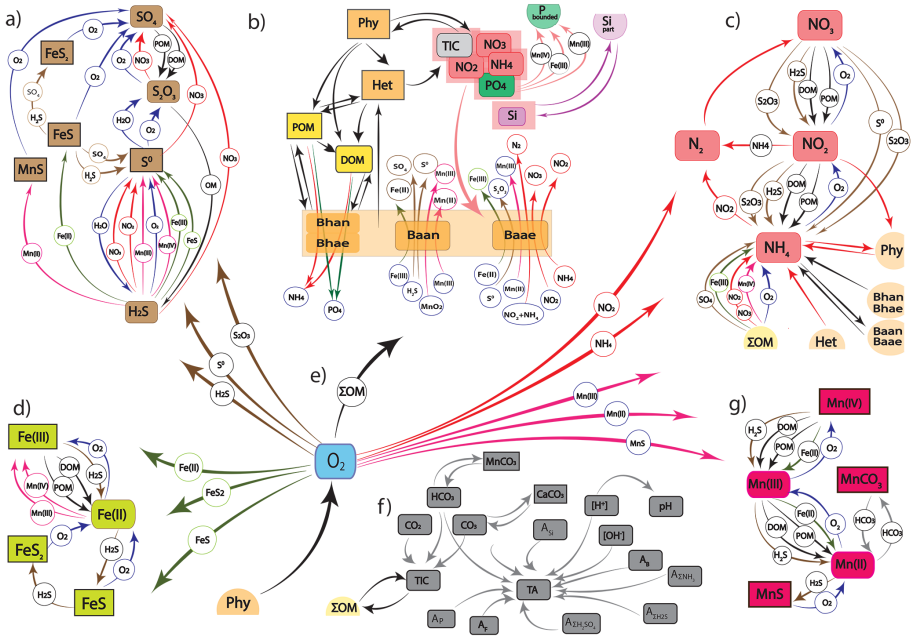

Figure 1. Flow-chart of biogeochemical processes represented in the Benthic RedOx Model (BROM). Transformation of sulphur species **(a)**, ecological block **(b)**, transformation of nitrogen species **(c)**, transformation of iron species **(d)**, processes affecting dissolved oxygen **(e)**, carbonate system and alkalinity **(f)**, transformation of manganese species **(g)**.

GMDD
doi:10.5194/gmd-2015-239

Bottom RedOx Model (BROM, v.1.0)

E. V. Yakushev et al.

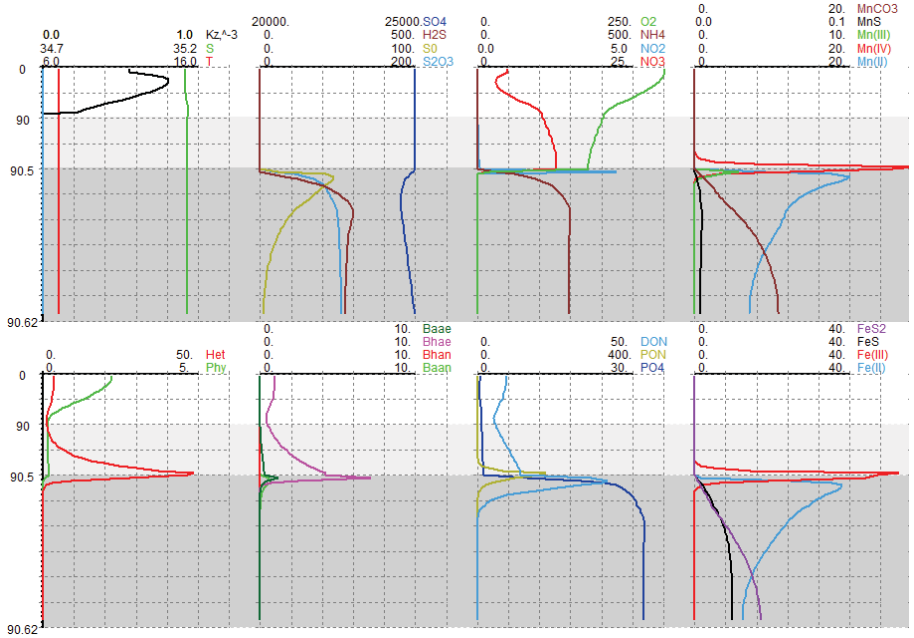

Figure 2. Vertical distributions of the modelled chemical parameters (µM), biological parameters (µM N), temperature (°C), salinity (PSU) and vertical transport coefficient (10^{-3} m^2 s^{-1}) in winter well-mixed conditions (day 90) in the water column 0–90 m (white background), the 50 cm thick BBL (90–90.5 m, light grey background) and 12 cm upper sediment pore water (90.5–90.62, dark grey background).

GMDD
doi:10.5194/gmd-2015-239

Bottom RedOx Model (BROM, v.1.0)

E. V. Yakushev et al.

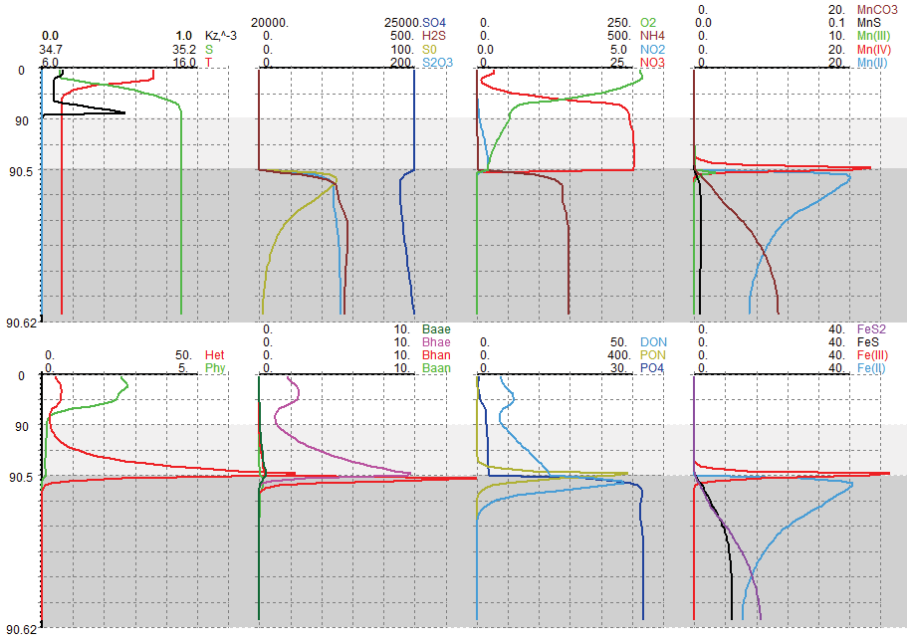

Figure 3. Vertical distributions of the modelled chemical parameters (μM), biological parameters (μM N), temperature (˚C), salinity (PSU) and vertical transport coefficient (10^{-3} m^2 s^{-1}) in the period of organic matter production and formation of pycnocline (day 215) in the water column 0–90 m (white background), the 50 cm thick BBL (90–90.5 m, light grey background) and 12 cm upper sediment pore water (90.5–90.62, dark grey background).

GMDD
doi:10.5194/gmd-2015-239

Bottom RedOx Model (BROM, v.1.0)

E. V. Yakushev et al.

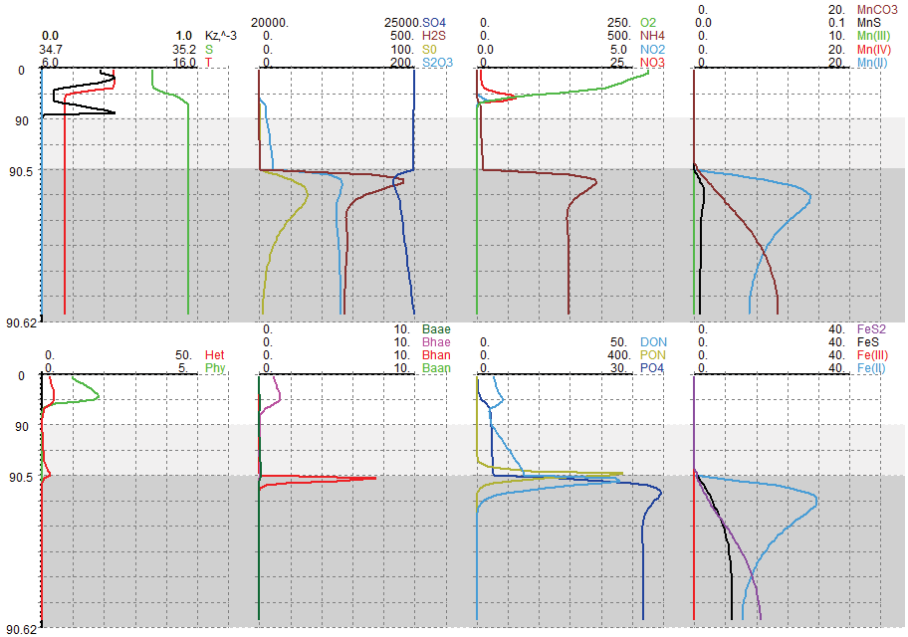

Figure 4. Vertical distributions of the modelled chemical parameters (μM), biological parameters (μM N), temperature (°C), salinity (PSU) and vertical transport coefficient (10^{-3} m^2 s^{-1}) in the period of stagnation and bottom anoxia (day 300) in the water column 0–90 m (white background), the 50 cm thick BBL (90–90.5 m, light grey background) and 12 cm upper sediment pore water (90.5–90.62, dark grey background).

GMDD
doi:10.5194/gmd-2015-239

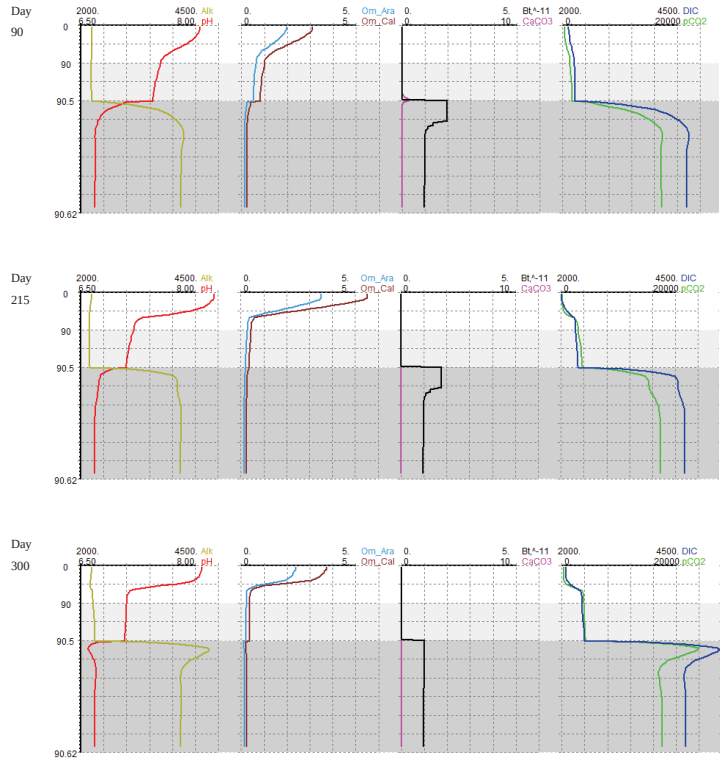

Figure 5. Vertical distributions of the modelled carbonate system parameters in the winter well-mixed conditions (day 90), in the period of organic matter production and formation of pycnocline (day 215) in the period of stagnation and bottom anoxia (day 300) in the water column 0–90 m (white background), the 50 cm thick BBL (90–90.5 m, light grey background) and 12 cm upper sediment pore water (90.5–90.62, dark grey background).

GMDD
doi:10.5194/gmd-2015-239

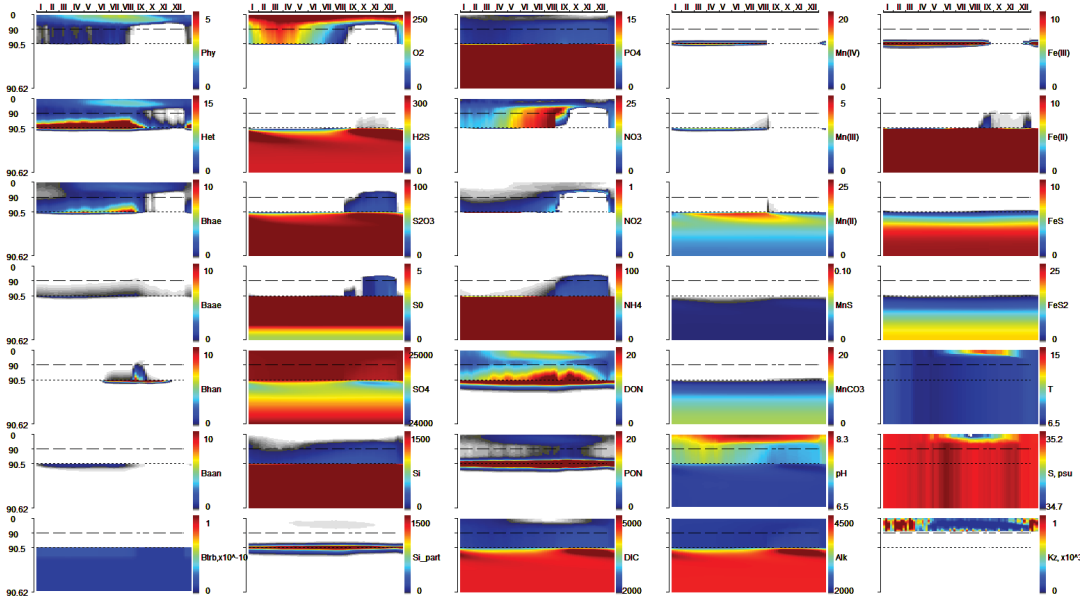

Figure 6. Simulated seasonal variability of the modelled chemical parameters (μM), biological parameters (μM N), temperature (°C), salinity (PSU) and vertical transport coefficient (10^{-3} m^2 s^{-1}). The dotted line corresponds to the sediment-BBL boundary and the dashed-line to the BBL-water column boundary.

GMDD
doi:10.5194/gmd-2015-239

Bottom RedOx Model (BROM, v.1.0)

E. V. Yakushev et al.

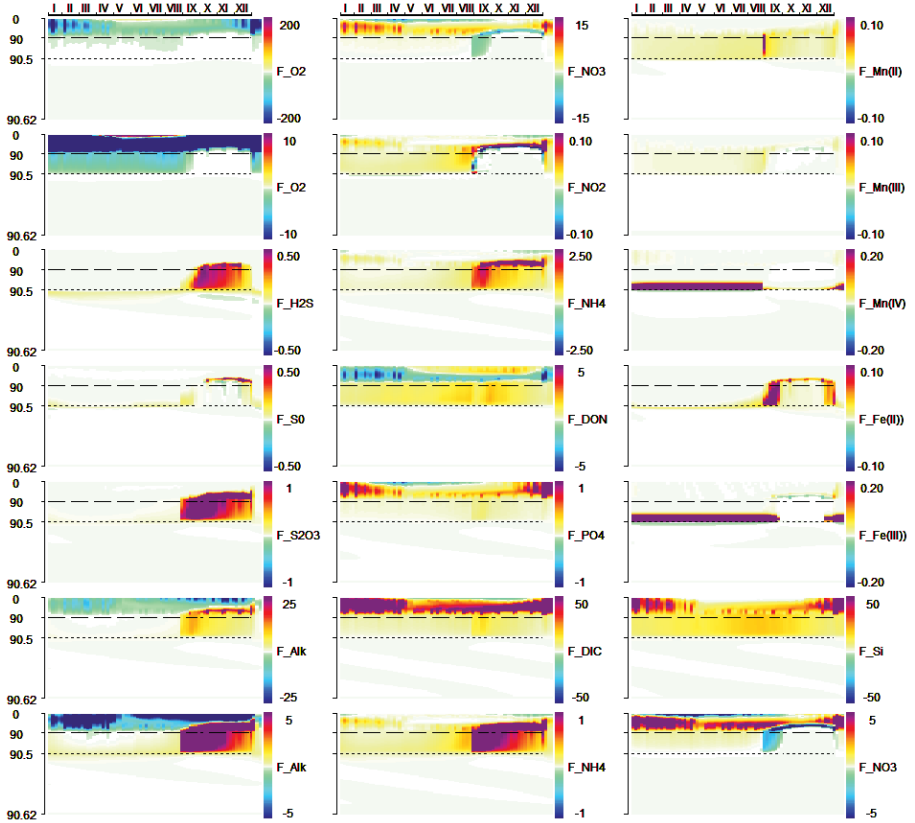

Figure 7. Simulated seasonal variability of vertical fluxes of oxygen, nitrate, Mn(IV), Mn(III), Fe(III), hydrogen sulphide, phosphate, ammonia, thiosulphate and elemental sulphur, directed upwards (∧) or downwards (v) in mmol m^2 d^{-1}.

GMDD
doi:10.5194/gmd-2015-239

Bottom RedOx Model (BROM, v.1.0)

E. V. Yakushev et al.

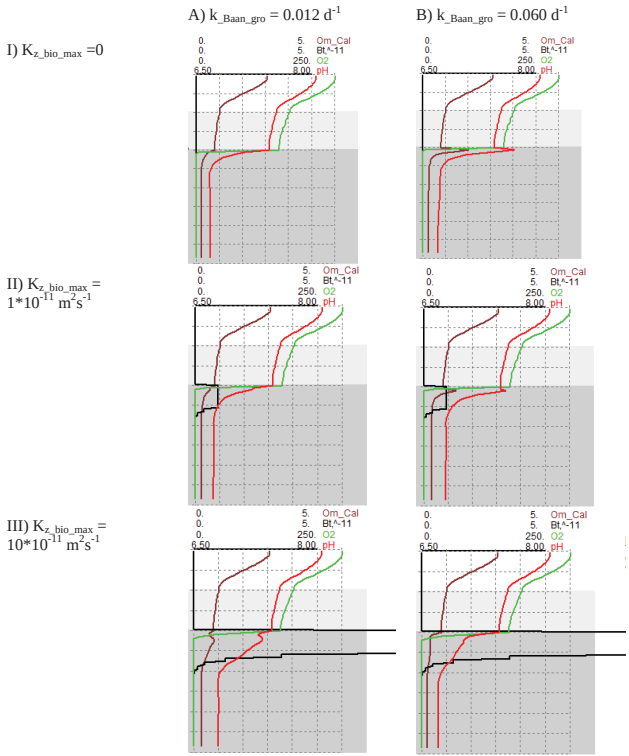

Figure 8. Modelled vertical distributions of O_2, pH, calcite saturation (Om_Ca) and Bioturbation (Bt) in day 90, winter: top row for (i) absence of bioturbation, (ii) baseline rates of bioturbation Kz_bio = 1×10^{-11} m^2 s^{-1} and (iii) overpriced rate of bioturbation Kz_bio = 10×10^{-11} m^2 s^{-1}. Left column correspond to baseline chemosynthesis **(a)** k_Baan_gro = 0.012 d^{-1} and increased chemosynthesis **(b)** k_Baan_gro = 0.060 d^{-1}.

GMDD
doi:10.5194/gmd-2015-239